# Interaction between periodic elastic waves and two contact nonlinearities

Stéphane Junca, Bruno Lombard

Mathematical Models and Methods in Applied Sciences


# INTERACTION BETWEEN PERIODIC ELASTIC WAVES AND TWO CONTACT NONLINEARITIES

STÉPHANE JUNCA
*Laboratoire J.A. Dieudonné, UMR 6621 CNRS, Université de Nice Sophia-Antipolis, Parc Valrose, 06108 Nice Cedex 02, France*
*junca@math.unice.fr*

BRUNO LOMBARD
*Laboratoire de Mécanique et d'Acoustique, UPR 7051 CNRS, 31 chemin Joseph Aiguier, 13402 Marseille, France*
*lombard@lma.cnrs-mrs.fr*

Received (Day Month Year)
Revised (Day Month Year)
Communicated by (xxxxxxxxxx)

Propagation of elastic waves is studied in a 1D medium containing two cracks. The latter are modeled by smooth nonlinear jump conditions accounting for the finite, non-null compressibility of real cracks. The evolution equations are written in the form of a system of two nonlinear neutral delay differential equations, leading to a well-posed Cauchy problem. Perturbation analysis indicates that, under periodic excitation, the periodic solutions oscillate around positive mean values, which increase with the forcing level. This typically nonlinear phenomenon offers non-destructive means to evaluate the cracks. Existence, uniqueness and attractivity of periodic solutions is then examined. At some particular values of the ratio between the wave travel time and the period of the source, results are obtained whatever the forcing level. With a much larger set of ratios but at small forcing levels, results are obtained under a Diophantine condition. Lastly, numerical experiments are proposed to illustrate the behavior of the periodic diffracted waves.

*Keywords*: elastic waves; nonlinear jump conditions; neutral delay differential equations; periodic solutions.

AMS Subject Classification: 34A12, 34C60, 35L04, 74J20

## 1. Introduction

### 1.1. *Physical motivation*

Studies on the interactions between ultrasonic waves and contact defects have crucial applications in the field of mechanics, especially as far as the nondestructive testing of materials is concerned. When the cracks are much smaller than the wavelengths, they are usually replaced by interfaces with appropriate jump conditions. Linear models for contact have been widely developed.[30] However, there is a cur-

rent tendency to develop nonlinear model in order to characterize the cracks more closely.

From the physical point of view, the simplest nonlinear model for crack is that involving unilateral contact.[31,36] In this non-smooth model, it is assumed that the region of imperfect contact cannot be compressed. A similar approach with a simplified piecewise linear model is studied in Ref. 20. More sophisticated smooth models, involving finite non-null crack compressibility, have been developed for applications to engineering[2] and geomechanical problems.[5]

The interaction of elastic waves with a contact nonlinearity has been addressed numerically and theoretically by various authors.[31,8,23,24] In Ref. 19, a detailed analysis was performed in the case of a single crack. It was established that a periodic excitation generates periodic diffracted waves; in addition, the jump in the elastic displacement across the crack has a positive mean value, contrary to what occurs in the case of linear models for contact, where the mean value is null. This jump, which increases strictly with the forcing level, amounts to a mean dilatation of the crack. It was quantified in terms of the parameters involved in the problem, which leads to potential acoustical means of determining the nonlinear properties of the crack.

The physical motivation of the present article is to examine whether the properties found to exist in the case of a single crack also apply to cases involving two cracks. Is there a couple of periodic solution with positive mean values ? As we will see, this is true under suitable conditions, but how to estimate these quantities ? It is a first step in the direction of a larger number of cracks, which frequently occurs in practical situations.

### 1.2. *Mathematical motivation*

Even under this simple generalization, the mathematical analysis is much more intricate than in Ref. 19, where one tackled with a ordinary differential equation. The successive reflections of waves between the cracks are described mathematically by a system of two nonlinear neutral-delay differential equation (NDDE) with periodic forcing.[15] The main features of this system are already contained in the following scalar NDDE:

$$x^{'}(t) + a\, x^{'}(t-1) + b\, f\,(x(t)) = s(t), \tag{1.1}$$

where $f$ is a smooth increasing nonlinear function, $f(0) = 0$, $f^{'}(0) = 1$, $|a| \leq 1, b > 0$ and $s$ is a periodic excitation. The existence and uniqueness of periodic solutions to (1.1) is not a trivial question when $|a| = 1$, which is the case encountered here. To our knowledge, articles and reference books dealing with forced NDDE and oscillation theory of delay equations, such as Refs. 25, 11, 9, 29, 13, 12, always consider the case $|a| < 1$. In the critical case $|a| = 1$ indeed, the difficulties follow from the very weak stability of periodic solutions: if we consider a null forcing $s = 0$ and a linear function $f(x) = x$, then elementary calculations show that the null solution is asymptotically stable but not exponentially stable.

The mathematical motivation of the present article is to analyze the existence and uniqueness of periodic solutions in this critical case, where the standard techniques cannot be applied.[7,10,25] We prove that periodic solutions of the linearized NDDE always exist, but also that they lose one order of regularity in some cases described by a Diophantine condition. In these cases, the existence and uniqueness of solutions to the original nonlinear NDDE may be lost. The results obtained here are relevant in other situations, where coupled systems are described by boundary conditions with finite-velocity traveling waves.[15]

### 1.3. *Sketch of the study*

The present paper is organized as follows:

- In section 2, the physical problem is stated in terms of linear hyperbolic partial differential equations and nonlinear jump conditions. It is transformed into a system of neutral delay differential equations which can be studied more easily;
- In section 3, the neutral Cauchy problem is adimensionalized. Existence and uniqueness of global solutions is proved. A qualitative result is given about the mean values of periodic solutions, or equivalently about the mean dilatations of the cracks;
- In section 4, perturbation analysis is performed. Analytic expressions are obtained for the mean dilatations of each cracks, which makes it possible to use an acoustic approach to estimate the nonlinear parameters of the cracks. The quantitative findings obtained on a single crack in Ref. 19 are thus extended to two cracks;
- In section 5, the existence and uniqueness of periodic solutions are proved whatever the amplitude of the source, but only at specific values of the ratio between the wave propagation time and the period of the source. Upper bounds of the solution are determined, and the geometrical properties of the configuration space are analyzed;
- In section 6, existence and uniqueness of periodic solutions are proved for a larger set of periods, by assuming a small source and a Diophantine condition on the ratio travel time / period of the source. Contrary to what occurs with a single crack, the periodic solutions are not exponentially stable in this case. The focus is put on the spectrum of the linearized system and on the localization of the small divisors.[18] The results obtained are then transferred to the nonlinear system;
- In section 7, numerical methods are introduced. Numerical simulations illustrate the qualitative properties of the scattered waves;
- In section 8, future lines of research are suggested: in one hand, the general case of $N$ cracks could be investigated, and on the other hand, other strategies could be developed for proving the existence and uniqueness of global solutions for a full set of periods and large forcing levels.

## 2. Problem statement

### 2.1. *Physical modeling*

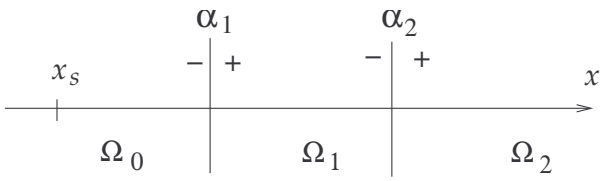


Fig. 1. Cracks at $\alpha_1$ and $\alpha_2$ in elastic media $\Omega_i$; source at $x_s < \alpha_1$.

Let us take two cracks at $\alpha_1$ and $\alpha_2$ in the linearly elastic media $\Omega_0$, $\Omega_1$ and $\Omega_2$ (figure 1). The density $\rho$ and the elastic speed of the compressional waves $c$ are positive, piecewise constant, and they may be discontinuous across the cracks.

Elastic compressional waves are emitted by a source at $x = x_s < \alpha_1$ in $\Omega_0$, and then they are diffracted by the cracks. Wave propagation is modeled by the 1-D linear elastodynamics[1]

$$\rho \frac{\partial v}{\partial t} = \frac{\partial \sigma}{\partial x}, \qquad \frac{\partial \sigma}{\partial t} = \rho c^2 \frac{\partial v}{\partial x} + S(t)\,\delta(x - x_s), \tag{2.1}$$

where $v = \frac{\partial u}{\partial t}$ is the elastic velocity, $u$ is the elastic displacement, and $\sigma$ is the elastic stress. The source $S(t)$ is causal, $T$-periodic, and it oscillates around a null mean value: otherwise, the incident elastic displacement would increase linearly with $t$, which is physically meaningless. The magnitude of the source is described by the amplitude $v_0$ of the elastic velocity.

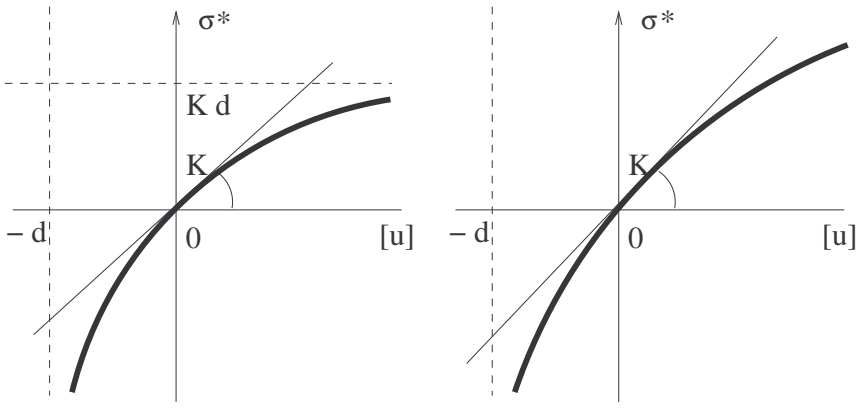


Fig. 2. Sketch of the nonlinear relation between the stress and the jump of the elastic displacement (2.5). Left row: model 1 (2.7), right row: model 2 (2.8).

Two independent jump conditions are required around each crack $\alpha_k$ $(k = 1, 2)$ to obtain a well-posed problem. First, the stress is assumed to be continuous across each crack[30]:

$$[\sigma(\alpha_k,\, t)] = 0 \;\Rightarrow\; \sigma(\alpha_k^+,\, t) = \sigma(\alpha_k^-,\, t) = \sigma_k^*(t). \tag{2.2}$$

Secondly, experimental and theoretical studies have yielded the following conclusions:

- the elastic displacement can be discontinuous across the cracks, depending on the stress applied;
- at small stress levels, a linear model is relevant

$$\sigma_k^*(t) = K_k\, [u(\alpha_k,\, t)]\,, \tag{2.3}$$

  where $K_k > 0$ is the *interfacial stiffness*[30,33];
- the jump in elastic displacement satisfies the inequality

$$[u(\alpha_k,\, t)] \geq -d_k, \tag{2.4}$$

  where $d_k > 0$ is the *maximum allowable closure.*[5] As the loading increases, the crack tends to become completely closed: $[u(\alpha_k,\, t)] \to -d_k^+$ when $\sigma_k^* \to -\infty$;
- concave stress-closure laws are measured.[26]

The relation

$$\sigma_k^*(t) = K_k\, d_k\, \mathcal{F}_k\left([u(\alpha_k,\, t)]/d_k\right) \tag{2.5}$$

satisfies these requirements, where $\mathcal{F}_k$ is a smoothly increasing concave function

$$\begin{aligned} &\mathcal{F}_k : ]-1,\, +\infty[ \to ]-\infty,\, \mathcal{F}_{k\,\max}[, \quad \lim_{X \to -1} \mathcal{F}_k(X) = -\infty, \quad 0 < \mathcal{F}_{k\,\max} \leq +\infty, \\ &\mathcal{F}_k(0) = 0, \quad \mathcal{F}_k^{'}(0) = 1, \quad \mathcal{F}_k^{''} < 0 < \mathcal{F}_k^{'}. \end{aligned} \tag{2.6}$$

Two models illustrate the nonlinear relation (2.5): the *model 1* proposed in Refs. 2, 5 writes

$$\sigma_k^*(t) = \frac{K_k\, [u(\alpha_k,\, t)]}{1 + [u(\alpha_k,\, t)]\,/d_k} \;\Leftrightarrow\; \mathcal{F}_k(X) = \frac{X}{1+X}, \quad \mathcal{F}_{k\,\max} = 1, \tag{2.7}$$

and the *model 2* proposed in Ref. 26 writes

$$\sigma_k^*(t) = K_k\, d_k\, \ln\left(1 + [u(\alpha_k,\, t)]/d_k\right) \;\Leftrightarrow\; \mathcal{F}_k(X) = \ln(1+X), \quad \mathcal{F}_{k\,\max} = +\infty. \tag{2.8}$$

These two models are sketched in figure 2. The straight line with a slope $K$ tangential to the curves at the origin gives the linear jump conditions (2.3).

### 2.2. *Reduction of the model*

We want to study the solution of the boundary-value problem stated in section 2.1. For this purpose, we focus on the jumps in the elastic displacements across the cracks $Y_k(t) = [u(\alpha_k,\, t)]$, where $k = 1,\, 2$: based on the method of characteristics, all the scattered fields can be deduced from the known 1-D Green's function and from these $Y_k(t)$. Moreover, it is simpler to study two functions of $t$ than the solution of partial differential equations.

In the next proposition, the problem stated in section 2.1 is reduced to a system of nonlinear *neutral delay differential equations* (NDDE), i.e. differential equations where the delay is included in the derivatives.[15]

**Proposition 2.1.** *Let us define the travel time* $\tau > 0$ *and the constants* $\beta_k > 0$ *and* $|\gamma_k| < \beta_k$ *(*$k = 1,\, 2$*)*

$$\begin{aligned}
&\tau = \frac{\alpha_2 - \alpha_1}{c_1},\\
&\beta_1 = K_1 \left( \frac{1}{\rho_0\, c_0} + \frac{1}{\rho_1\, c_1} \right), \quad \beta_2 = K_2 \left( \frac{1}{\rho_2\, c_2} + \frac{1}{\rho_1\, c_1} \right),\\
&\gamma_1 = K_1 \left( \frac{1}{\rho_0\, c_0} - \frac{1}{\rho_1\, c_1} \right), \quad \gamma_2 = K_2 \left( \frac{1}{\rho_2\, c_2} - \frac{1}{\rho_1\, c_1} \right).
\end{aligned} \tag{2.9}$$

*Then the jumps* $Y_k(t) = [u(\alpha_k,\, t)]$ *satisfy the system of NDDE*

$$\begin{cases}
\dfrac{d\, Y_1}{d\, t}(t) + \dfrac{d\, Y_2}{d\, t}(t-\tau) = -\beta_1\, d_1\, \mathcal{F}_1 \left( \dfrac{Y_1(t)}{d_1} \right) - \gamma_2\, d_2\, \mathcal{F}_2 \left( \dfrac{Y_2(t-\tau)}{d_2} \right) + \dfrac{1}{\rho_0\, c_0^2}\, S(t),\\[2ex]
\dfrac{d\, Y_2}{d\, t}(t) + \dfrac{d\, Y_1}{d\, t}(t-\tau) = -\beta_2\, d_2\, \mathcal{F}_2 \left( \dfrac{Y_2(t)}{d_2} \right) - \gamma_1\, d_1\, \mathcal{F}_1 \left( \dfrac{Y_1(t-\tau)}{d_1} \right) + \dfrac{1}{\rho_0\, c_0^2}\, S(t-\tau),\\[2ex]
Y_1(t) = Y_2(t) = 0 \;\; \textit{for} \;\; -\tau \leq t \leq 0.
\end{cases} \tag{2.10}$$

**Proof.** The proof is mainly based on the method of characteristics. In the first part, we collect results based on elastodynamics[1] and on the jump conditions (2.2) and (2.5). In each subdomain $\Omega_k$, the elastic displacement can be split into rightward moving (R) and leftward moving (L) waves

$$u(x,\, t) = u_{Rk} \left( t - \frac{x}{c_k} \right) + u_{Lk} \left( t + \frac{x}{c_k} \right),$$

where $u_{L2} = 0$: no leftward moving wave comes from $+\infty$. It follows that

$$\frac{\partial\, u}{\partial\, t}(x,\, t) = \begin{cases}
+c_k\, \dfrac{\partial\, u}{\partial\, x}(x,\, t) + 2\, u_{Rk}^{'} \left( t - \dfrac{x}{c_k} \right),\\[2ex]
-c_k\, \dfrac{\partial\, u}{\partial\, x}(x,\, t) + 2\, u_{Lk}^{'} \left( t + \dfrac{x}{c_k} \right),
\end{cases} \tag{2.11}$$

where $u_{L2}^{'} = 0$. The elastic stresses are

$$\sigma(x,\, t) = \rho_k\, c_k^2\, \frac{\partial\, u}{\partial\, x}(x,\, t). \tag{2.12}$$

The first jump condition (2.2) and the equation (2.12) yield

$$\rho_{k-1}\, c_{k-1}^2\, \frac{\partial\, u}{\partial\, x}(\alpha_k^-,\, t) = \rho_k\, c_k^2\, \frac{\partial\, u}{\partial\, x}(\alpha_k^+,\, t) = \sigma_k^*(t). \tag{2.13}$$

The second jump condition (2.5) and the equation (2.13) yield

$$\begin{cases} \dfrac{\partial\, u}{\partial\, x}(\alpha_k^-,\, t) = \dfrac{K_k\, d_k}{\rho_{k-1}\, c_{k-1}^2}\ \mathcal{F}_k\left(\dfrac{Y_k(t)}{d_k}\right), \\ \dfrac{\partial\, u}{\partial\, x}(\alpha_k^+,\, t) = \dfrac{K_k\, d_k}{\rho_k\, c_k^2}\ \mathcal{F}_k\left(\dfrac{Y_k(t)}{d_k}\right). \end{cases} \tag{2.14}$$

The rightward moving wave emitted by the source (2.1), which impacts the first crack at $\alpha_1$, is

$$u_{R0}^{'}\left(t - \frac{x}{c_0}\right) = -\frac{1}{2\,\rho_0\, c_0^2}\, S\,(t - t_s)\,, \tag{2.15}$$

where $t_s = (\alpha_1 - x_s)/c_0$. From (2.11), (2.14) and (2.15), the traces of $\frac{\partial\, u}{\partial\, t}$ can be deduced:

$$\begin{aligned} &\frac{\partial\, u}{\partial\, t}(\alpha_1^-,\, t) = \frac{K_1\, d_1}{\rho_0\, c_0}\, \mathcal{F}_1\left(\frac{Y_1(t)}{d_1}\right) - \frac{1}{\rho_0\, c_0^2}\, S\,(t - t_s)\,, \\ &\frac{\partial\, u}{\partial\, t}(\alpha_1^+,\, t) = \frac{d\, Y_1}{d\, t}(t) + \frac{K_1\, d_1}{\rho_0\, c_0}\, \mathcal{F}_1\left(\frac{Y_1(t)}{d_1}\right) - \frac{1}{\rho_0\, c_0^2}\, S\,(t - t_s)\,, \\ &\frac{\partial\, u}{\partial\, t}(\alpha_2^-,\, t) = -\frac{d\, Y_2}{d\, t}(t) - \frac{K_2\, d_2}{\rho_2\, c_2}\, \mathcal{F}_2\left(\frac{Y_2(t)}{d_2}\right). \end{aligned} \tag{2.16}$$

In the second part of the proof, we write the traces of rightward and leftward moving waves at $\alpha_1^+$ and $\alpha_2^-$. From (2.9), (2.11), (2.14) and (2.16), it follows

$$2\, u_{R1}^{'}\left(t - \frac{\alpha_1}{c_1}\right) = \frac{d\, Y_1}{d\, t}(t) + \gamma_1\, d_1\, \mathcal{F}_1\left(\frac{Y_1(t)}{d_1}\right) - \frac{1}{\rho_0\, c_0^2}\, S\,(t - t_s) \tag{2.17}$$

and

$$2\, u_{R1}^{'}\left(t - \frac{\alpha_2}{c_1}\right) = -\frac{d\, Y_2}{d\, t}(t) - \beta_2\, d_2\, \mathcal{F}_2\left(\frac{Y_2(t)}{d_2}\right). \tag{2.18}$$

The equality $u_{R1}^{'}(t - \alpha_1/c_1) = u_{R1}^{'}(t + \tau - \alpha_2/c_1)$ along with (2.17) and (2.18) yields

$$\frac{d\, Y_1}{d\, t}(t) + \frac{d\, Y_2}{d\, t}(t+\tau) = -\gamma_1\, d_1\, \mathcal{F}_1\left(\frac{Y_1(t)}{d_1}\right) - \beta_2\, d_2\, \mathcal{F}_2\left(\frac{Y_2(t+\tau)}{d_2}\right) + \frac{1}{\rho_0\, c_0^2}\, S\,(t - t_s)\,. \tag{2.19}$$

Likewise, it follows from (2.9), (2.11), (2.14) and (2.16)

$$2\, u_{L1}^{'}\left(t + \frac{\alpha_1}{c_1}\right) = \frac{d\, Y_1}{d\, t}(t) + \beta_1\, d_1\, \mathcal{F}_1\left(\frac{Y_1(t)}{d_1}\right) - \frac{1}{\rho_0\, c_0^2}\, S\left(t - \frac{\alpha_1 - x_s}{c_0}\right) \tag{2.20}$$

and

$$2\,u_{L1}^{'}\left(t+\frac{\alpha_2}{c_1}\right)=-\frac{d\,Y_2}{d\,t}(t)-\gamma_2\,d_2\,\mathcal{F}_2\left(\frac{Y_2(t)}{d_2}\right). \tag{2.21}$$

The equality $u_{L1}^{'}(t+\alpha_1/c_1)=u_{L1}^{'}(t-\tau+\alpha_2/c_1)$ along with (2.20) and (2.21) yields

$$\frac{d\,Y_1}{d\,t}(t)+\frac{d\,Y_2}{d\,t}(t-\tau)=-\beta_1\,d_1\,\mathcal{F}_1\left(\frac{Y_1(t)}{d_1}\right)-\gamma_2\,d_2\,\mathcal{F}_2\left(\frac{Y_2(t-\tau)}{d_2}\right)+\frac{1}{\rho_0\,c_0^2}\,S\,(t-t_s)\,. \tag{2.22}$$

Constants (2.9) are injected into (2.19) and (2.22); the time is shifted: $t-t_s\to t$; a time shift $t+\tau\to t$ is also applied to (2.19), which results in the system of NDDE (2.10). Lastly, the initial conditions follow from the causality of the source and from the finite propagation time between $x_s$ and $\alpha_1$. □

## 3. Neutral delay differential equations

### 3.1. *Cauchy problem*

Setting

$$\begin{array}{l}
y_1(t)=\dfrac{Y_1(t)}{d_1}=\dfrac{[u(\alpha_1,\,t)]}{d_1},\quad y_2(t)=\dfrac{Y_2(t)}{d_1}=\dfrac{[u(\alpha_2,\,t)]}{d_1},\quad r=\dfrac{d_2}{d_1}>0,\\
v_0=\dfrac{1}{2\,\rho_0\,c_0^2}\,\max\limits_{[0,\,T]}S(t),\quad S(t)=2\,v_0\,\rho_0\,c_0^2\sum\limits_{n=-\infty}^{+\infty}s_n\,e^{i\,n\,\omega\,t},\quad s_0=0,\quad s(t)=\dfrac{1}{d_1\,\rho_0\,c_0^2}\,S(t),\\
f_1(y)=-\mathcal{F}_1(y),\;f_2(y)=-r\,\mathcal{F}_2\left(\dfrac{y}{r}\right),\;f_{k\,\min}=-\mathcal{F}_{k\,\max}<0,\;y_{1\,\min}=-1,\;y_{2\,\min}=-r,
\end{array} \tag{3.1}$$

the system (2.9)-(2.10) leads to the Cauchy problem

$$\begin{cases}
y_1^{'}(t)+y_2^{'}(t-\tau)=\beta_1\,f_1(y_1(t))+\gamma_2\,f_2(y_2(t-\tau))+s(t), & t>0,\\
y_2^{'}(t)+y_1^{'}(t-\tau)=\beta_2\,f_2(y_2(t))+\gamma_1\,f_1(y_1(t-\tau))+s(t-\tau), & t>0,\\
y_k(t)=\phi_k(t)\in C^1\left([-\tau,\,0],\,]y_{k\,\min},\,+\infty[\right), & -\tau\le t\le 0.
\end{cases} \tag{3.2}$$

Contrary to what occurred in (2.10), the initial data $\phi_k$ may differ from 0. Assumptions and new notations are defined as follows ($k=1,\,2$):

$$\begin{array}{l}
\beta_k>0,\quad 0\le|\gamma_k|<\beta_k,\quad y_{k\,\min}<0,\\
f_k\in C^2\left(]y_{k\,\min},\,+\infty[\to]f_{k\,\min},\,+\infty[\right),\quad \lim\limits_{y\to y_{k\,\min}}f_k(y)=+\infty,\quad -\infty\le f_{k\,\min}<0,\\
f_k(0)=0,\quad f_k^{'}(0)=-1,\quad q_k=\dfrac{f_k^{''}(0)}{2}>0,\quad f_k^{'}(y)<0<f_k^{''}(y),\\
s\in C^0(\mathbb{R}),\quad s(t+T)=s(t),\quad t>0,\quad T>0,\quad \omega=2\,\pi\,/\,T,\quad \varphi=\omega\,\tau.
\end{array} \tag{3.3}$$

The inequality $0 \leq |\gamma_k| < \beta_k$ in (3.3) follows from (2.9) and is of crucial importance in following analysis. The reciprocal functions $f_k^{-1}$ satisfy

$$\begin{aligned} &f_k^{-1} \in C^2\left(]f_{k\min}, +\infty[\rightarrow]y_{k\min}, +\infty[\right), \qquad \lim_{y\rightarrow+\infty} f_k^{-1}(y) = y_{k\min}, \\ &f_k^{-1}(0) = 0, \quad \left(f_k^{-1}\right)' < 0 < \left(f_k^{-1}\right)''. \end{aligned} \tag{3.4}$$

In the case of model 1 (2.7), we obtain

$$f_k(y) = f_k^{-1}(y) = -\frac{y}{1-\frac{y}{y_{k\min}}}, \quad f_{k\min} = y_{k\min}. \tag{3.5}$$

In the case of model 2 (2.8), we obtain

$$f_k(y) = y_{k\min}\,\ln\left(1-\frac{y}{y_{k\min}}\right), \quad f_k^{-1}(y) = -y_{k\min}\,\left(\exp\left(\frac{y}{y_{k\min}}\right)-1\right), \quad f_{k\min} = -\infty. \tag{3.6}$$

The causal source is often taken to be monochromatic: $s_{\pm1} = \mp i\,/\,2$ and $s_{i\neq\pm1} = 0$ in (3.1), and thus

$$S(t) = 2\,v_0\,\rho_0\,c_0^2\,\sin\omega\,t, \qquad t \geq 0. \tag{3.7}$$

Lastly, the ratio between the travel time and the period of the source is introduced

$$\theta = \frac{\tau}{T} = \frac{\alpha_2-\alpha_1}{c_1\,T} = \frac{\alpha_2-\alpha_1}{\lambda_1} > 0, \tag{3.8}$$

where $\lambda_1$ is the wavelength in medium $\Omega_1$.

### 3.2. *Global solutions*

In this section, we prove the existence and uniqueness of solutions to the Cauchy problem (3.2)-(3.3). We begin with an elementary result about global solutions for ODE.

**Lemma 3.1.** *Let $\tau > 0$, $g \in C^0\left([0,\,\tau],\,\mathbb{R}\right)$, and the scalar non-autonomous ODE*

$$\begin{cases} y'(t) = f(y(t)) + g(t), \\ y(0) = y_0, \end{cases} \tag{3.9}$$

*where $f \in C^1\left(]y_{\min}, +\infty[,\,]f_{\min}, +\infty[\right)$, $f(0) = 0$, $f' < 0$ and $y_0 > y_{\min}$. The unique maximal solution is therefore also a global solution: $y \in C^1\left([0,\,\tau],\,]y_{\min}, +\infty[\right)$.*

**Proof.** Two cases are distinguished.
Case 1: $0 \leq \sup g < |f_{\min}|$. The constants $a < b$ are taken to be such that

$$f(a) = -\inf g, \qquad f(b) = -\sup g.$$

If $y_{\min} < y < a$, then $f(y) > -\inf g$ and thus $y' > 0$; on the contrary, $y > b$ means that $y' < 0$. Consequently, $[a,\,b]$ is a *funnel*[17]: if $y_0$ belongs to this compact set, then $y$ remains trapped inside. Otherwise, the solution will be found in $[a,\,b]$ in finite

time. In both configurations, the solution remains bounded, therefore it is a global solution.
Case 2: $\sup g \geq |f_{\min}|$. If $y > 0$, then $y^{'} < g(t)$ and

$$y(t) < y_0 + \int_0^t g(\xi)\, d\xi < y_0 + t \sup g.$$

In $[0,\, \tau]$, $y$ is thus bounded by the upper solution $y_0 + \tau \sup g$, which concludes the proof. □

Now, we prove the existence of global solutions $y_1$ and $y_2$ to (3.2)-(3.3) that satisfy $y_k > y_{k\min}$. This inequality was required by the model of contact: see (2.4) and (3.1).

**Proposition 3.1.** *There exists a unique solution* $\mathbf{y} = (y_1,\, y_2)^T$ *to (3.2)-(3.3), with* $y_k \in C^1\left([0,\, +\infty[,\, ]y_{k\min},\, +\infty[\right)$*, except at instants* $t = k\,\tau$*,* $k \in \mathbb{N}$*, where the derivatives may be discontinuous.*

**Proof.** The proof is performed by induction, according to the *step method*: see for instance the proof of theorems 2-1 or 7-1 in Ref. 15. Intervals $I_k = [k\,\tau,\, (k+1)\,\tau]$, $k = -1,\, 0,\, 1, ...$ are defined. In $I(-1)$, the following explicit solutions exist: $y_k(t) = \phi_k(t) > y_{k\min}$. The couple of solutions is therefore assumed to be known in $I_k$, $k \geq 0$, and to satisfy the statements made in proposition 3.1. In $I_{k+1}$, the system (3.2) is written

$$\begin{cases} y_1^{'}(t) = \beta_1\, f_1(y_1(t)) - y_2^{'}(t-\tau) + \gamma_2\, f_2(y_2(t-\tau)) + s(t), & t \in I_{k+1}, \\ \\ y_2^{'}(t) = \beta_2\, f_2(y_2(t)) - y_1^{'}(t-\tau) + \gamma_1\, f_1(y_1(t-\tau)) + s(t-\tau), & t \in I_{k+1}. \end{cases}$$

In the latter system, the right-hand terms $\beta_k\, f(y_k(t))$ satisfy the assumptions made in lemma 3.1. Since $y_k^{'}(t-\tau)$ in $I_{k+1}$ are equal to $y_k^{'}(t)$ on $I_k$, the other terms on the right-hand side are continuous, which concludes the proof. □

### 3.3. *Mean values of periodic solutions*

No general proof of the existence and uniqueness of periodic solutions to (3.2)-(3.3) have been obtained whatever the amplitude of the periodic source $s$ and the ratio $\theta$ in (3.8). In section 5, we give results valid for any source but for particular values of $\theta$. In section 6, a larger set of $\theta$ is studied, but the source is small.

**Remark 3.1.** If there exists a $T$-periodic solution $\mathbf{y} = (y_1,\, y_2)^T$, then replacing $\tau$ by $\tau + T$, i.e. $\theta$ by $\theta + 1$, does not affect the system (3.2). The study of periodic solutions can therefore be restricted to $\theta \in ]0,\, 1]$.

Assuming that a $T$-periodic regime has been reached, the solution can be written as Fourier series

$$y_k(t) = \sum_{n=-\infty}^{+\infty} y_k^{(n)}\, e^{i\,n\,\omega\,t}, \qquad k = 1, 2. \tag{3.10}$$

Since the source is real, the coefficients satisfy $y_k^{(-n)} = \widehat{y_k^{(n)}}$, where the hat refers to the conjugate. The following proposition concerns the mean value of the solution during one period, which is denoted by an overline

$$\overline{y_k} = y_k^{(0)} = \frac{1}{T}\int_0^T y_k(t)\,dt, \qquad k = 1, 2. \tag{3.11}$$

**Proposition 3.2.** *The mean values of periodic solution* $\mathbf{y} = (y_1,\, y_2)^T$ *to (3.2)-(3.3) are strictly positive:*

$$\overline{y_k} > 0, \qquad k = 1, 2. \tag{3.12}$$

**Proof.** $T$-periodicity of the solution and of the source in (3.2) yields

$$\begin{cases} \beta_1\, \overline{f_1(y_1(t))} + \gamma_2\, \overline{f_2(y_2(t-\tau))} = 0, \\ \gamma_1\, \overline{f_1(y_1(t-\tau))} + \beta_2\, \overline{f_2(y_2(t))} = 0. \end{cases}$$

The mean value of a periodic function is invariant by a time shift of the function, thus

$$\begin{cases} \beta_1\, \overline{f_1(y_1(t))} + \gamma_2\, \overline{f_2(y_2(t))} = 0, \\ \gamma_1\, \overline{f_1(y_1(t))} + \beta_2\, \overline{f_2(y_2(t))} = 0. \end{cases}$$

The bounds in (3.3) mean that the determinant of the linear system is non-null: $\Delta = \beta_1\,\beta_2 - \gamma_1\,\gamma_2 > 0$. Therefore, one obtains

$$\overline{f_1(y_1(t))} = 0, \qquad \overline{f_2(y_2(t))} = 0.$$

Jensen's inequality applied to the convex functions $f_1$ and $f_2$ yields

$$f_1(\overline{y_1}) < 0, \qquad f_2(\overline{y_2}) < 0.$$

The properties of $f_k$ in (3.3) are used to conclude the proof. □

Proposition 3.2 means that the jump of elastic displacement across each crack $Y_k = [u(\alpha_k,\, t)] = d_1\, y_k$ has a positive mean value $\overline{Y_k} > 0$. In other words, there is a mean dilatation of each crack when a periodic source is excited, as in the case of a single crack.[19] This property has been observed both experimentally,[21] and it is illustrated numerically in section 7.2. Quantitative analysis is proposed in section 4; physical implications are addressed in section 8.1.

**Remark 3.2.** Numerical simulations indicate that $\theta \to \overline{y_k}(\theta)$ is 0.5-periodic, i.e. that it shows half of the periodicity of the solution $y_k$ (see remark 3.1). No rigorous proof of this statement have been obtained so far, however, except in the case of small forcing levels: see section 4.2 and figure 8.

## 4. Perturbation analysis

Throughout this section, it will be assumed that there exists a unique periodic solution $\mathbf{y} = (y_1,\, y_2)^T$ to (3.2)-(3.3), which depends smoothly on the forcing level, and especially on the ratio $v_0 \,/\, d_1$. This assumption will be validated in section 6 for a dense set of ratio $\theta$, as stated in theorem 6.1 and proposition 6.1.

In the case of small solutions, a second-order Taylor expansion of the NDDE system gives

$$\begin{cases} y_1^{'}(t) + y_2^{'}(t-\tau) + \beta_1\, y_1(t) - \beta_1\, q_1\, y_1^2(t) + \gamma_2\, y_2(t-\tau) - \gamma_2\, q_2\, y_2^2(t-\tau) \\ \qquad\qquad +\mathcal{O}\left(y_1^3(t) + y_2^3(t-\tau)\right) = \dfrac{2\, v_0}{d_1} \displaystyle\sum_{n=-\infty}^{+\infty} s_n\, e^{i\, n\, \omega\, t}, \\ y_2^{'}(t) + y_1^{'}(t-\tau) + \beta_2\, y_2(t) - \beta_2\, q_2\, y_2^2(t) + \gamma_1\, y_1(t-\tau) - \gamma_1\, q_1\, y_1^2(t-\tau) \\ \qquad\qquad +\mathcal{O}\left(y_1^3(t-\tau) + y_2^3(t)\right) = \dfrac{2\, v_0}{d_1} \displaystyle\sum_{n=-\infty}^{+\infty} s_n\, e^{i\, n\, \omega\, t}\, e^{-i\, n\, \varphi}. \end{cases} \tag{4.1}$$

The previous uniqueness assumption ensures that the solution can be sought in the form

$$y_k = y_{k(1)} + y_{k(2)} + \mathcal{O}\left(\left(\frac{v_0}{d_1\, \omega}\right)^3\right), \qquad |y_{k(2)}| \ll |y_{k(1)}| \ll 1. \tag{4.2}$$

Injecting (4.2) into (4.1) provides a set of recursive linear NDDE systems which are easy to solve. Before detailing the resolution in sections 4.1 and 4.2, an elementary technical result is introduced.

**Lemma 4.1.** *Let us take the notations defined in section 3.1. Then, for all* $n \in \mathbb{N}^*$,

$$\Delta_n = \left(1 - i\, \frac{\beta_1}{n\, \omega}\right)\, \left(1 - i\, \frac{\beta_2}{n\, \omega}\right) - \left(1 - i\, \frac{\gamma_1}{n\, \omega}\right)\, \left(1 - i\, \frac{\gamma_2}{n\, \omega}\right)\, e^{-2\, i\, n\, \varphi} \neq 0. \tag{4.3}$$

**Proof.** Since $\beta_k > |\gamma_k|$ in (3.3), we obtain

$$\left|1 - i\, \frac{\beta_1}{n\, \omega}\right|\, \left|1 - i\, \frac{\beta_2}{n\, \omega}\right| > \left|1 - i\, \frac{\gamma_1}{n\, \omega}\right|\, \left|1 - i\, \frac{\gamma_2}{n\, \omega}\right|,$$

and thus

$$\left|\left(1 - i\, \frac{\beta_1}{n\, \omega}\right)\, \left(1 - i\, \frac{\beta_2}{n\, \omega}\right)\right| > \left|\left(1 - i\, \frac{\gamma_1}{n\, \omega}\right)\, \left(1 - i\, \frac{\gamma_2}{n\, \omega}\right)\, e^{-2\, i\, n\, \varphi}\right|,$$

which concludes the proof. □

### 4.1. *First-order solution*

The first-order terms in (4.1)-(4.2) are collected, resulting in

$$\begin{cases} y_{1(1)}^{'}(t) + y_{2(1)}^{'}(t-\tau) + \beta_1\, y_{1(1)}(t) + \gamma_2\, y_{2(1)}(t-\tau) = \dfrac{2\,v_0}{d_1} \displaystyle\sum_{n=-\infty}^{+\infty} s_n\, e^{i\,n\,\omega\,t}, \\ y_{2(1)}^{'}(t) + y_{1(1)}^{'}(t-\tau) + \beta_2\, y_{2(1)}(t) + \gamma_1\, y_{1(1)}(t-\tau) = \dfrac{2\,v_0}{d_1} \displaystyle\sum_{n=-\infty}^{+\infty} s_n\, e^{i\,n\,\omega\,t}\, e^{-i\,n\,\varphi}. \end{cases} \tag{4.4}$$

Fourier series

$$y_{k(1)} = \sum_{n=-\infty}^{+\infty} y_{k(1)}^{(n)}\, e^{i\,n\,\omega\,t}, \qquad k = 1, 2, \tag{4.5}$$

are injected into (4.4), and similar trigonometric arguments are then put together. The constant terms satisfy the linear system

$$\begin{cases} \beta_1\, y_{1(1)}^{(0)} + \gamma_2\, y_{2(1)}^{(0)} = 0, \\ \gamma_1\, y_{1(1)}^{(0)} + \beta_2\, y_{2(1)}^{(0)} = 0, \end{cases} \tag{4.6}$$

which involves a non-null determinant $\beta_1\,\beta_2 - \gamma_1\,\gamma_2 > 0$, and thus

$$y_{1(1)}^{(0)} = y_{2(1)}^{(0)} = 0. \tag{4.7}$$

The first-order solution therefore oscillates around a null-mean value. Collecting the $e^{i\,n\,\omega\,t}$ terms gives the linear system

$$\begin{cases} \left(1 - i\,\dfrac{\beta_1}{n\,\omega}\right)\, y_{1(1)}^{(n)} + \left(1 - i\,\dfrac{\gamma_2}{n\,\omega}\right)\, e^{-i\,n\,\varphi}\, y_{2(1)}^{(n)} = -i\,\dfrac{2\,v_0}{d_1\,\omega}\,\dfrac{s_n}{n}, \\ \left(1 - i\,\dfrac{\gamma_1}{n\,\omega}\right)\, e^{-i\,n\,\varphi}\, y_{1(1)}^{(n)} + \left(1 - i\,\dfrac{\beta_2}{n\,\omega}\right)\, y_{2(1)}^{(n)} = -i\,\dfrac{2\,v_0}{d_1\,\omega}\,\dfrac{s_n}{n}\, e^{-i\,n\,\varphi}, \end{cases} \tag{4.8}$$

the determinant of which is $\Delta_n \neq 0$ (see (4.3)). Setting

$$\begin{aligned} X_{1(1)}^{(n)} &= \frac{\left(1 - i\,\dfrac{\gamma_2}{n\,\omega}\right)\, e^{-2\,i\,n\,\varphi} - \left(1 - i\,\dfrac{\beta_2}{n\,\omega}\right)}{\left(1 - i\,\dfrac{\beta_1}{n\,\omega}\right)\, \left(1 - i\,\dfrac{\beta_2}{n\,\omega}\right) - \left(1 - i\,\dfrac{\gamma_1}{n\,\omega}\right)\, \left(1 - i\,\dfrac{\gamma_2}{n\,\omega}\right)\, e^{-2\,i\,n\,\varphi}}, \\ X_{2(1)}^{(n)} &= \frac{i\,\dfrac{\beta_1 + \gamma_1}{n\,\omega}\, e^{-i\,n\,\varphi}}{\left(1 - i\,\dfrac{\beta_1}{n\,\omega}\right)\, \left(1 - i\,\dfrac{\beta_2}{n\,\omega}\right) - \left(1 - i\,\dfrac{\gamma_1}{n\,\omega}\right)\, \left(1 - i\,\dfrac{\gamma_2}{n\,\omega},\right)\, e^{-2\,i\,n\,\varphi}}, \end{aligned} \tag{4.9}$$

the non-constant first-order solutions are

$$y_{1(1)}^{(n)} = i\,\frac{2\,v_0}{d_1\,\omega}\, X_{1(1)}^{(n)}\,\frac{s_n}{n}, \qquad y_{2(1)}^{(n)} = i\,\frac{2\,v_0}{d_1\,\omega}\, X_{2(1)}^{(n)}\,\frac{s_n}{n}, \qquad n \neq 0. \tag{4.10}$$

### 4.2. *Second-order solution*

The second-order terms in (4.1)-(4.2) are collected, resulting in

$$\begin{cases} y_{1(2)}^{'}(t) + y_{2(2)}^{'}(t-\tau) + \beta_1\, y_{1(2)}(t) + \gamma_2\, y_{2(2)}(t-\tau) = \beta_1\, q_1\, y_{1(1)}^2(t) + \gamma_2\, q_2\, y_{2(1)}^2(t-\tau), \\ y_{2(2)}^{'}(t) + y_{1(2)}^{'}(t-\tau) + \beta_2\, y_{2(2)}(t) + \gamma_1\, y_{1(2)}(t-\tau) = \beta_2\, q_2\, y_{2(1)}^2(t) + \gamma_1\, q_1\, y_{1(1)}^2(t-\tau). \end{cases} \tag{4.11}$$

Fourier series

$$y_{k(2)} = \sum_{n=-\infty}^{+\infty} y_{k(2)}^{(n)}\, e^{i\,n\,\omega\,t}, \qquad k = 1, 2, \tag{4.12}$$

are injected into (4.11), and similar trigonometric arguments are then put together. From (4.7), the following linear system satisfied by the constant terms

$$\begin{cases} \beta_1\, y_{1(2)}^{(0)} + \gamma_2\, y_{2(2)}^{(0)} = 2\,\beta_1\, q_1 \displaystyle\sum_{n=1}^{+\infty} \left| y_{1(1)}^{(n)} \right|^2 + 2\,\gamma_2\, q_2 \sum_{n=1}^{+\infty} \left| y_{2(1)}^{(n)} \right|^2, \\ \gamma_1\, y_{1(2)}^{(0)} + \beta_2\, y_{2(2)}^{(0)} = 2\,\gamma_1\, q_1 \displaystyle\sum_{n=1}^{+\infty} \left| y_{1(1)}^{(n)} \right|^2 + 2\,\beta_2\, q_2 \sum_{n=1}^{+\infty} \left| y_{2(1)}^{(n)} \right|^2 \end{cases} \tag{4.13}$$

is obtained, the determinant of which is $\beta_1\,\beta_2 - \gamma_1\,\gamma_2 > 0$. The system is solved by using first-order solutions (4.10), which gives the constant second-order terms

$$y_{k(2)}^{(0)} = 8\, q_k \left( \frac{v_0}{d_1\,\omega} \right)^2 \sum_{n=1}^{+\infty} \left| X_{k(1)}^{(n)} \right|^2 \left| \frac{s_n}{n} \right|^2, \qquad k = 1, 2. \tag{4.14}$$

Unlike first-order solutions, second-order solutions oscillate around non-null mean values. The consequence on the jumps of elastic displacements $Y_k = [u(\alpha_k,\, t)] = d_1\, y_k$ is stated in the next proposition.

**Proposition 4.1.** *At small forcing level, and using $X_{k(1)}^{(n)}$ defined in (4.9), the mean values of the $T$-periodic jumps $Y_k$ are*

$$\overline{Y_k} = \frac{\left| \mathcal{F}_k^{''}(0) \right|}{d_k} \left( \frac{v_0}{\omega} \right)^2 \sum_{n=1}^{+\infty} \left| X_{k(1)}^{(n)} \right|^2 \left| \frac{s_n}{n} \right|^2 + \mathcal{O}\left( \frac{v_0^3}{d_1^2\,\omega^3} \right), \qquad k = 1,\, 2. \tag{4.15}$$

**Proof.** From (3.1) and (3.3), it follows

$$q_1 = \frac{f_1^{''}(0)}{2} = \frac{|\mathcal{F}_1^{''}(0)|}{2}, \qquad q_2 = \frac{f_2^{''}(0)}{2} = \frac{d_1}{d_2}\, \frac{|\mathcal{F}_2^{''}(0)|}{2}. \tag{4.16}$$

Putting together (3.1), (4.2), (4.5) and (4.12) yields second-order estimates of $\overline{Y_k}$

$$\overline{Y_k} = d_1 \left( y_{k(1)}^{(0)} + y_{k(2)}^{(0)} + \mathcal{O}\left( \left( \frac{v_0}{d_1\,\omega} \right)^3 \right) \right), \qquad k = 1, 2. \tag{4.17}$$

Injecting (4.7), (4.14) and (4.16) into (4.17) gives an estimate value of $\overline{Y_k}$. □

To conclude the perturbation analysis, higher-order expansions than (4.2) could be investigated. However, the contributions of third-order and higher-order might yield divergent estimates of $\overline{Y_k}$ in the case of large forcing levels.[23] In practice, the second-order expansion suffices for this purpose. As shown in section 7.3, equation (4.2) yields highly accurate estimates of the mean dilatations $\overline{Y_k}$. The physical relevance of these quantities is discussed in section 8.1.

## 5. Periodic solutions: special cases

### 5.1. *Existence and uniqueness*

In this section, the analytical results will be expressed successively in terms of the coefficients of the model problem (3.2), and in terms of the physical parameters (preceded by the sign $\equiv$).

To begin with, we assume that $\tau$ is a period of $s$: $\tau = n\,T$, and thus $\theta = n \in \mathbb{N}^*$ in (3.8). This amounts to saying that $\Omega_1$ contains $n$ wavelengths of the source.

**Theorem 5.1.** *If $\theta = n \in \mathbb{N}^*$, then there exists a unique periodic solution $\mathbf{y} = (y_1,\, y_2)^T$ to (3.2)-(3.3) having the same period $T$ as the source. In addition, the increasing diffeomorphism*

$$G(y) = f_2^{-1}\left(\frac{\beta_1 - \gamma_1}{\beta_2 - \gamma_2}\, f_1(y)\right) \equiv f_2^{-1}\left(\frac{K_1}{K_2}\, f_1(y)\right), \qquad G^{'} > 0, \qquad G(0) = 0, \tag{5.1}$$

*ensures that*

$$y_2(t) = G\left(y_1(t)\right). \tag{5.2}$$

*Lastly, $y_1$ and $y_2$ satisfy a scalar non autonomous ODE without any delay.*

**Proof.** Injecting $\tau$-periodic solutions $y_k$ into (3.2) yields a system of ODE

$$\begin{cases} y_1^{'}(t) + y_2^{'}(t) = \beta_1\, f_1(y_1(t)) + \gamma_2\, f_2(y_2(t)) + s(t), \\ y_2^{'}(t) + y_1^{'}(t) = \beta_2\, f_2(y_2(t)) + \gamma_1\, f_1(y_1(t)) + s(t), \end{cases} \tag{5.3}$$

and therefore

$$(\beta_2 - \gamma_2)\, f_2(y_2(t)) = (\beta_1 - \gamma_1)\, f_1(y_1(t)).$$

From (2.9), we obtain

$$f_2(y_2(t)) = \frac{\beta_1 - \gamma_1}{\beta_2 - \gamma_2}\, f_1(y_1(t)) \equiv \frac{K_1}{K_2}\, f_1(y_1(t)), \tag{5.4}$$

which gives (5.2). The ranges of the left-hand and right-hand sides in (5.4) may be different. To obtain the bijective relation (5.2), the domain of definition of $G$ in (5.1) has to be examined carefully, as done further in the corollary 5.1. Equation (5.2) is then injected into (5.3), which gives the ODE

$$H(y_1)^{'} = K(y_1) + s(t), \tag{5.5}$$

where $H$ is an increasing diffeomorphism

$$H(y) = y + G(y), \quad H(0) = 0, \quad H^{'} > 0,$$

and $K$ is a decreasing diffeomorphism (see (3.3), (2.9)):

$$K(y) = k\, f_1(y),$$

$$k = \beta_1 + \gamma_2\, \frac{\beta_1 - \gamma_1}{\beta_2 - \gamma_2} = \gamma_1 + \beta_2\, \frac{\beta_1 - \gamma_1}{\beta_2 - \gamma_2} \equiv K_1 \left( \frac{1}{\rho_0\, c_0} + \frac{1}{\rho_2\, c_2} \right) > 0.$$

Taking $z_1 = H(y_1)$ and (5.5), we obtain the non autonomous ODE

$$z_1^{'} = L(z_1) + s(t), \tag{5.6}$$

where $L$ is a decreasing diffeomorphism

$$L = K \circ H^{-1}, \quad L(0) = 0.$$

The existence and uniqueness of a $T$-periodic solution to (5.6) follows from the global asymptotic stability of the solution $z_1 = 0$ at null forcing level, which is induced by the properties of $L$. A similar case has been investigated in propositions 4-1 and 6-1 of Ref. 19. By construction, $y_1 = H^{-1}(z_1)$ and $y_2 = G \circ H^{-1}(z_1)$ are also $T$-periodic solutions to (3.2). $\square$

The case where $2\,\tau$ is an odd period of $s$ can be treated in a similar way: $2\,\tau = (2\,n + 1)\,T$, $n \in \mathbb{N}$. This amounts to saying that $\Omega_1$ contains $n$ and a half wavelengths of the source.

**Theorem 5.2.** *If $\theta = n + 1/2$ with $n \in \mathbb{N}$, then there exists a unique periodic solution $\mathbf{y} = (y_1,\, y_2)^T$ to (3.2)-(3.3) having the same period $T$ as the source. In addition, the diffeomorphism (5.1) ensures that*

$$y_2(t) = G\left(y_1(t - T/2)\right). \tag{5.7}$$

*Lastly, $y_1$ and $y_2$ satisfy a scalar non autonomous ODE without any delay.*

**Proof.** A time shift $t \to t + \tau$ is applied to the first equation of (3.2)

$$\begin{cases} y_1^{'}(t+\tau) + y_2^{'}(t) = \beta_1\, f_1(y_1(t+\tau)) + \gamma_2\, f_2(y_2(t)) + s(t+\tau), \\ \\ y_2^{'}(t) + y_1^{'}(t-\tau) = \beta_2\, f_2(y_2(t)) + \gamma_1\, f_1(y_1(t-\tau)) + s(t-\tau). \end{cases}$$

The $2\,\tau$-periodic solutions to (3.2) therefore satisfy

$$(\beta_2 - \gamma_2)\, f_2(y_2(t)) = (\beta_1 - \gamma_1)\, f_1(y_1(t-\tau)),$$

hence

$$y_2(t) = G\left(y_1(t-\tau)\right). \tag{5.8}$$

The rest of the proof follows on exactly the same lines as the proof of theorem 5.1, proving the existence and uniqueness of $T$-periodic solutions $(y_1,\, y_2)$. We therefore obtain

$$y_1(t-\tau) = y_1(t-(n+1/2)\,T),$$

$$= y_1(t-T/2),$$

which simplifies (5.8) into (5.7). □

Some comments are required about theorems 5.1 and 5.2:

- The relations (5.2) and (5.7) can be expressed in a single formula: if $\theta = n/2$ and $n \in \mathbb{N}$, then
$$y_2(t) = G\left(y_1(t-t_0)\right), \tag{5.9}$$
where $t_0 = 0$ if $n$ is even, $t_0 = T/2$ otherwise.
- With model 1 (3.5) and model 2 (3.6), $G$ can be determined exactly
$$\text{model 1: } G(y) = \frac{\beta_1-\gamma_1}{\beta_2-\gamma_2}\,\frac{y}{1+\left(1-\dfrac{1}{r}\,\dfrac{\beta_1-\gamma_1}{\beta_2-\gamma_2}\right)y} \equiv \frac{K_1}{K_2}\,\frac{y}{1+\left(1-\dfrac{K_1\,d_1}{K_2\,d_2}\right)y},$$
$$\text{model 2: } G(y) = r\left((1+y)^{\dfrac{1}{r}\,\dfrac{\beta_1-\gamma_1}{\beta_2-\gamma_2}}-1\right) \equiv \frac{d_2}{d_1}\left((1+y)^{\dfrac{K_1\,d_1}{K_2\,d_2}}-1\right). \tag{5.10}$$
- $G$ has a crucial effect on the qualitative properties of $(y_1,\, y_2)$, which makes it necessary to analyze this function more closely. This is the goal of the next proposition.

**Proposition 5.1.** *The diffeomorphism $G$ (5.1) is the identity $I$ if and only if the cracks are identical:*

$$\begin{aligned} G = I &\Leftrightarrow \beta_1-\gamma_1 = \beta_2-\gamma_2, \quad r=1, \quad f_1 = f_2, \\ &\Leftrightarrow K_1 = K_2, \quad d_1 = d_2, \quad \mathcal{F}_1 = \mathcal{F}_2. \end{aligned} \tag{5.11}$$

**Proof.** Assuming $G = I$ amounts to

$$(\beta_1-\gamma_1)\,f_1(y) = (\beta_2-\gamma_2)\,f_2(y),$$

for all $y$ in the domain in which $G$ is valid. By differentiation, we obtain

$$(\beta_1-\gamma_1)\,f_1^{'}(y) = (\beta_2-\gamma_2)\,f_2^{'}(y) \;\Rightarrow\; (\beta_1-\gamma_1)\,f_1^{'}(0) = (\beta_2-\gamma_2)\,f_2^{'}(0).$$

Since $f_k^{'}(0) = -1$, it follows that $\beta_1-\gamma_1 = \beta_2-\gamma_2$, or equivalently $K_1 = K_2$. The injectivity of $f_1$ and $f_2$ means that $f_1 = f_2$, and thus (3.1) yields

$$\mathcal{F}_1(y) = r\,\mathcal{F}_1\left(\frac{y}{r}\right).$$

The latter equation is differentiated twice, and then it is evaluated at 0:

$$\mathcal{F}_1^{''}(0) = \frac{1}{r}\,\mathcal{F}_1^{''}(0).$$

Since the concavity of the contact laws are non null at the origin (2.6), $r = d_2/d_1 = 1$. The reciprocal of the proof is trivial. □

### 5.2. *Upper bounds*

At some values of $f_{k\,\min}$ in (3.3), upper bounds $y_k \leq y_{k\,\max}$ can be deduced from (5.9), as stated in the following corollary.

**Corollary 5.1.** *Let $\theta = n/2$ with $n \in \mathbb{N}$, and*

$$\xi = \frac{\beta_2 - \gamma_2}{\beta_1 - \gamma_1}\left|\frac{f_{2\,\min}}{f_{1\,\min}}\right| \equiv \frac{K_2}{K_1}\left|\frac{f_{2\,\min}}{f_{1\,\min}}\right|.$$

*Four cases are distinguished:*

*(1) $f_{1\,\min} > -\infty$, $f_{2\,\min} > -\infty$: one solution may be bounded*

- $\xi < 1 \Rightarrow y_{1\,\max} = f_1^{-1}\left(-\dfrac{\beta_2-\gamma_2}{\beta_1-\gamma_1}\,|f_{2\,\min}|\right) \equiv f_1^{-1}\left(-\dfrac{K_2}{K_1}\,|f_{2\,\min}|\right), \quad y_{2\,\max} = +\infty,$
- $\xi = 1 \Rightarrow y_{1\,\max} = y_{2\,\max} = +\infty,$
- $\xi > 1 \Rightarrow y_{2\,\max} = f_2^{-1}\left(-\dfrac{\beta_1-\gamma_1}{\beta_2-\gamma_2}\,|f_{1\,\min}|\right) \equiv f_2^{-1}\left(-\dfrac{K_1}{K_2}\,|f_{1\,\min}|\right), \quad y_{1\,\max} = +\infty,$

*(2) $f_{1\,\min} > -\infty$, $f_{2\,\min} = -\infty$: one upper bound exists*

$$y_{2\,\max} = f_2^{-1}\left(-\frac{\beta_1-\gamma_1}{\beta_2-\gamma_2}\,|f_{1\,\min}|\right) \equiv f_2^{-1}\left(-\frac{K_1}{K_2}\,|f_{1\,\min}|\right), \quad y_{1\,\max} = +\infty,$$

*(3) $f_{1\,\min} = -\infty$, $f_{2\,\min} > -\infty$: one upper bound exists*

$$y_{1\,\max} = f_1^{-1}\left(-\frac{\beta_2-\gamma_2}{\beta_1-\gamma_1}\,|f_{2\,\min}|\right) \equiv f_1^{-1}\left(-\frac{K_2}{K_1}\,|f_{2\,\min}|\right), \quad y_{2\,\max} = +\infty,$$

*(4) $f_{1\,\min} = -\infty$, $f_{2\,\min} > -\infty$: no upper bound exists.*

$$y_{1\,\max} = y_{2\,\max} = +\infty.$$

**Proof.** In (5.9), the diffeomorphism $G : ]y_{1\,\min},\, y_{2\,\max}[ \to ]y_{2\,\min},\, y_{2\,\max}[$ satisfies

$$\begin{aligned}\frac{\beta_1-\gamma_1}{\beta_2-\gamma_2}\,f_1(y_{1\,\max}) = f_2(y_{2\,\max}) &= \max\left(\frac{\beta_1-\gamma_1}{\beta_2-\gamma_2}\,f_{1\,\min},\, f_{2\,\min}\right),\\ &= -\min\left(\frac{\beta_1-\gamma_1}{\beta_2-\gamma_2}\,|f_{1\,\min}|\,,\,|f_{2\,\min}|\right).\end{aligned} \tag{5.12}$$

Knowing whether (5.12) can be solved or not leads to the four cases distinguished in corollary 5.1. Here, we deal only with case 1: the proof of the other cases follows exactly the same lines. Solving (5.12) requires to solve

$$f_1(y_{1\,\max}) = -\,|f_{1\,\min}|\,\min\left(1,\,\frac{\beta_2-\gamma_2}{\beta_1-\gamma_1}\left|\frac{f_{2\,\min}}{f_{1\,\min}}\right|\right) = \Delta_1. \tag{5.13}$$

If $\Delta_1 < f_{1\,\min}$, then (5.13) cannot be solved, and $y_{1\,\max} = +\infty$. On the contrary,

$$\Delta_1 > f_{1\,\min} \Leftrightarrow \frac{\beta_2 - \gamma_2}{\beta_1 - \gamma_1} \left| \frac{f_{2\,\min}}{f_{1\,\min}} \right| < 1$$

leads to the bounded value $y_{1\,\max}$ given in case 1. □

Model 2 (3.6) corresponds to case 4, where no upper bound exists, whereas model 1 (3.5) corresponds to case 1, where an upper bounds may exist. From (3.1), we obtain

$$\begin{aligned}
&\xi = r\,\frac{\beta_2 - \gamma_2}{\beta_1 - \gamma_1} \equiv \frac{K_2\,d_2}{K_1\,d_1},\\
&* \quad \xi < 1 \;\Rightarrow\; y_{1\,\max} = \frac{1}{1/\xi - 1}, \qquad y_{2\,\max} = +\infty,\\
&* \quad \xi = 1 \;\Rightarrow\; y_{1\,\max} = y_{2\,\max} = +\infty\\
&* \quad \xi > 1 \;\Rightarrow\; y_{2\,\max} = \frac{r}{\xi - 1}, \qquad y_{1\,\max} = +\infty.
\end{aligned}$$

### 5.3. *Configuration space*

Lastly, we deal with the geometrical features of the configuration space. Taking any increasing diffeomorphism $f$, we define the closed curve

$$\Gamma_f : \left| \begin{array}{l} [0,\,T] \to \mathbb{R}^2 \\ t \mapsto (f(y_1(t)),\, y_2(t))\,. \end{array} \right. \tag{5.14}$$

**Proposition 5.2.** *Let us consider the increasing diffeomorphism $G$ in (5.1). If $\theta = n + 1/2$, $n \in \mathbb{N}$, then*

- *$\Gamma_G$ (5.14) is symmetrical with respect to the first bisecting line;*
- *if the source is monochromatic (3.7), then $\Gamma_G$ contains a unique double point on this bisecting line.*

*If $\theta = n \in \mathbb{N}^*$, then $\Gamma_G$ is a segment on the first bisecting line.*

**Proof.** The case $\theta = n$ is a straightforward consequence of (5.2) and (5.14). In the case $\theta = n + 1/2$, theorem 5.2 yields

$$\begin{cases} G(y_1(t + T/2)) = G(y_1(t - T/2)) = y_2(t), \\ y_2(t + T/2) = G(y_1(t)). \end{cases}$$

The study of $\Gamma_G$ can therefore be restricted to $[0,\,T/2]$. On $[T/2,\,T]$, $\Gamma_G$ is obtained by permuting $G(y_1)$ and $y_2$, which amounts to performing a symmetry with respect to the line $y_2 = G(y_1)$, i.e. the first bisecting line.

On the other hand, the phase portrait of the solution to (5.6) in the case of a monochromatic source has been studied extensively in section 4 of Ref. 19: the

solution behaves like a distorted sinus. Since $H$ and $G \circ H^{-1}$ are diffeomorphisms, $y_1$ and $y_2$ show the same pattern of evolution. Theorem 5.2 ensures that $G(y_1(t))$ and $y_2(t)$ are $T$-periodic and equal, with a time shift $T/2$. They therefore cross twice at the same value, which concludes the proof. □

## 6. Periodic solution: small forcing

### 6.1. *Main result*

We take $H_T^p$ to denote the Sobolev space of $T$-periodic functions of square integrable on a period, with their derivatives up to order $p$; in particular, $H_T^0 = L_T^2$.

Unlike the special cases investigated in section 5, the main result obtained in this section involves a much larger set of values of ratios $\theta = \tau \,/\, T$, where $\tau$ is the travel time between the cracks and $T$ is the period of the source. To quantify this set, the following definition is introduced.

**Definition 6.1 (Diophantine condition $\mathcal{D}$).** *Let*

$$\zeta = \frac{\beta_1 - \gamma_1 + \beta_2 - \gamma_2}{4\,\pi^2}\,\tau > 0. \tag{6.1}$$

*A real number $w \in \mathbb{R}^+$ does not satisfy the condition $\mathcal{D}$ if and only if there exists an infinite number of integers $(n,\, k)$ such that*

$$2\,w = \frac{n}{k} + \frac{\zeta}{w}\,\frac{1}{k^2} + o\left(\frac{1}{k^2}\right). \tag{6.2}$$

Condition $\mathcal{D}$ in definition 6.1 is stated as a negative statement. An equivalent positive statement is given by condition $\mathcal{P}$ in proposition 6.3 stated further. Condition $\mathcal{D}$ is optimal to avoid a small divisor problem.[28,18] Assuming that $\mathcal{D}$ is true and considering a small source $s$, the following local existence and uniqueness results are obtained.

**Theorem 6.1.** *Let $\theta = \tau \,/\, T$ satisfy the Diophantine condition $\mathcal{D}$. Then there exists a neighborhood $V_s \times V_1 \times V_2$ of the origin in $\left(H_T^1\right)^3$ such that for any $s$ in $V_s$, there exists a unique periodic solution $\mathbf{y} = (y_1,\, y_2)^T = \mathbf{\Psi}(s)$ to (3.2)-(3.3) on $V_1 \times V_2$. This solution has the same period $T$ as the source, and $\mathbf{\Psi} \in C^1\left(V_s,\, V_1 \times V_2\right)$.*

Theorem 6.1 is proved in section 6.5. An example of a dense set satisfying $\mathcal{D}$ is given in the next proposition, proved in section 6.4.

**Proposition 6.1.** *If $\theta$ is rational, then $\mathcal{D}$ is satisfied. As a consequence, the conclusions of theorem 6.1 hold.*

### 6.2. *Spectrum of the linearized system*

In the case of small solutions, the system (3.2)-(3.3) is linearized, which leads to

$$\begin{cases} y_1^{'}(t) + y_2^{'}(t-\tau) + \beta_1\, y_1(t) + \gamma_2\, y_2(t-\tau) = s(t), \\ \\ y_2^{'}(t) + y_1^{'}(t-\tau) + \beta_2\, y_2(t) + \gamma_1\, y_1(t-\tau) = s(t-\tau). \end{cases} \tag{6.3}$$

Taking

$$\begin{aligned} &\mathbf{y}(t) = \begin{pmatrix} y_1 \\ y_2 \end{pmatrix}, \quad \mathbf{s}(t) = \begin{pmatrix} s(t) \\ s(t-\tau) \end{pmatrix}, \\ &\mathbf{A} = \begin{pmatrix} 0 & 1 \\ 1 & 0 \end{pmatrix}, \quad \mathbf{B} = \begin{pmatrix} \beta_1 & 0 \\ 0 & \beta_2 \end{pmatrix}, \quad \mathbf{C} = \begin{pmatrix} 0 & \gamma_2 \\ \gamma_1 & 0 \end{pmatrix}, \end{aligned} \tag{6.4}$$

the system (6.3) can be written in the following matrix form:

$$\mathcal{L}\,\mathbf{y}(t) = \mathbf{y}^{'}(t) + \mathbf{A}\,\mathbf{y}^{'}(t-\tau) + \mathbf{B}\,\mathbf{y}(t) + \mathbf{C}\,\mathbf{y}(t-\tau) = \mathbf{s}(t). \tag{6.5}$$

We are looking for solutions of the homogeneous system obtained by taking $\mathbf{s} = \mathbf{0}$ in (6.5). Injecting $\mathbf{y}(t) = \mathbf{y}_0\, e^{\Lambda\, t}$ where $\mathbf{y}_0$ is a constant vector, it follows $\mathbf{H}(\Lambda)\,\mathbf{y}_0 = \mathbf{0}$, where $\mathbf{H}$ is the matrix

$$\mathbf{H}(\Lambda) = \begin{pmatrix} \Lambda + \beta_1 & e^{-\Lambda\,\tau}\,(\Lambda + \gamma_2) \\ \\ e^{-\Lambda\,\tau}\,(\Lambda + \gamma_1) & \Lambda + \beta_2 \end{pmatrix}. \tag{6.6}$$

Nontrivial solutions are obtained iff $\det \mathbf{H} = 0$, and thus $\Lambda$ is a root of the characteristic equation

$$h(\Lambda) = (\Lambda + \beta_1)\,(\Lambda + \beta_2) - e^{-2\,\Lambda\,\tau}(\Lambda + \gamma_1)\,(\Lambda + \gamma_2) = 0. \tag{6.7}$$

The position of characteristic roots of (6.7) plays a decisive role on the stability of the neutral system. As shown in the next proposition, the neutral system (6.5) with coefficients (6.4) is a critical case not investigated in Refs. 7, 15.

**Proposition 6.2.** *The following results hold for the characteristic roots of (6.7):*

*(1) the roots are located in a vertical strip* $\Lambda_{\inf} < \Re\mathrm{e}\ \Lambda < 0$ *in the complex plane;*
*(2) a real negative root* $\Lambda_0$ *exists;*
*(3) the set of roots of* $h$ *is countable infinite;*
*(4) the roots* $\Lambda$ *tend towards the imaginary axis:* $\Re\mathrm{e}\ \Lambda \to 0$ *as* $|\Lambda| \to +\infty$.

*The neutral system (6.5) is therefore stable but not exponentially stable.*

**Proof.** Part 1. As $\Re\mathrm{e}\ \Lambda \to +\infty$, $h(\Lambda) \sim \Lambda^2$ which does not vanish. Likewise, $\Re\mathrm{e}\ \Lambda \to -\infty$ means that $e^{2\,\Lambda\,\tau}\,h(\Lambda) \sim -\Lambda^2$, and $h(\Lambda)$ therefore does not vanish, and we obtain

$$-\infty < \Lambda_{\inf} < \Re\mathrm{e}\ \Lambda < \Lambda_{\sup} < +\infty.$$

In addition, the characteristic roots $\Lambda$ satisfy

$$|\Lambda + \beta_1||\Lambda + \beta_2| = e^{-2\,\Re\mathrm{e}\ \Lambda}\,|\Lambda + \gamma_1||\Lambda + \gamma_2|. \tag{6.8}$$

If $\Re\mathrm{e}\ \Lambda \geq 0$, then $e^{-2\,\Re\mathrm{e}\ \Lambda} \leq 1$, thus

$$|\Lambda+\beta_1||\Lambda+\beta_2| \leq |\Lambda+\gamma_1||\Lambda+\gamma_2|,$$

which is impossible, because of (3.3): and therefore $\Re\mathrm{e}\ \Lambda < 0$.

Part 2. The properties

$$h(0) = \beta_1\,\beta_2 - \gamma_1\,\gamma_2 > 0, \qquad \lim_{x\to-\infty} h(x) = -\infty$$

ensure the existence of a negative real solution $\Lambda_0$.

Part 3. Let $z = 1\,/\,(2\,\Lambda\,\tau)$. Since $h(0) \neq 0$, $h(\Lambda) = 0$ is equivalent to $g(z) = 0$, where

$$g(z) = e^{\frac{1}{z}}\,r(z) - 1, \qquad r(z) = \frac{(1+2\,\tau\,\beta_1\,z)\ (1+2\,\tau\,\beta_2\,z)}{(1+2\,\tau\,\gamma_1\,z)\ (1+2\,\tau\,\gamma_2\,z)}.$$

Based on part 2, $z_0 = 1\,/\,(2\,\Lambda_0\,\tau)$ is a root of $g$: 0 belongs to the image of $g$. Lastly, $g$ is holomorphic on $\mathbb{C}$, except at the essential singularity 0. The Great Picard theorem therefore states that $g$ takes the value 0 infinitely often.

Part 4. Since $h$ is holomorphic, it has a finite number of roots on each compact. Points 1 and 3 therefore mean that $|\Im\mathrm{m}\ \Lambda| \to +\infty$. On the other hand, it follows from (6.8) that $e^{-2\,\Re\mathrm{e}\ \Lambda} \sim 1$ when $|\Im\mathrm{m}\ \Lambda| \to +\infty$, and hence $\Re\mathrm{e}\ \Lambda \to 0$: $\Lambda_{\mathrm{sup}} = 0$ is an accumulation point, and the system (6.5) is stable but not exponentially stable.[37] $\square$

Based on proposition 6.2 (first part), there exists a unique periodic solution to the linear system of NDDE (6.3) whatever the ratio $\theta = \tau\,/\,T$. A finer analysis of the characteristic roots $\Lambda$ of (6.7) is now needed to determine the smoothness of this solution. It is crucial indeed for obtaining existence and uniqueness results about the original nonlinear NDDE (3.2), as seen in section 6.5. The next lemma constitutes a first step in this direction.

**Lemma 6.1.** *For large values of $|\Lambda|$, there exists $n \in \mathbb{Z}^*$ such that $\Lambda$ is close to $i\,\frac{n\,\pi}{\tau}$. More precisely, this characteristic roots denoted by $\Lambda_n$ satisfies the following asymptotic expansion:*

$$\Lambda_n = i\,\left(\frac{n\,\pi}{\tau} + \frac{\beta_1-\gamma_1+\beta_2-\gamma_2}{2\,n\,\pi}\right) - \frac{\tau}{(2\,n\,\pi)^2}\,\left(\beta_1^2-\gamma_1^2+\beta_2^2-\gamma_2^2\right) + \mathcal{O}\left(\frac{1}{n^3}\right). \tag{6.9}$$

*At sufficiently large values of $n > 0$, the real and imaginary parts of $\Lambda_n$ increase strictly with $n$ (if $n < 0$, the imaginary parts of $\Lambda_n$ decrease strictly with $n$).*

**Proof.** If $\Lambda$ is a root of (6.7), and if $|\Lambda| \to +\infty$, then

$$e^{2\,\Lambda\,\tau} = \frac{(\Lambda+\gamma_1)\ (\Lambda+\gamma_2)}{(\Lambda+\beta_1)\ (\Lambda+\beta_2)} \sim 1. \tag{6.10}$$

Consequently, there exists $z_n$ tending towards 0 as $n$ increases and such that

$$\Lambda \equiv \Lambda_n = i\,\frac{n\,\pi}{\tau} + z_n. \tag{6.11}$$

To estimate $z_n$, (6.11) is injected into the characteristic equation (6.7), which gives

$$\begin{aligned} & e^{2\,z_n\,\tau}\left(i + \frac{\tau}{n\,\pi}\,(z_n + \beta_1)\right)\left(i + \frac{\tau}{n\,\pi}\,(z_n + \beta_2)\right) \\ & \quad - \left(i + \frac{\tau}{n\,\pi}\,(z_n + \gamma_1)\right)\left(i + \frac{\tau}{n\,\pi}\,(z_n + \gamma_2)\right) = 0. \end{aligned} \tag{6.12}$$

The equation (6.12) is satisfied with the discrete variable $n$; it is now extended to the continuous variable $u = \tau\,/\,(n\,\pi)$, and we take $z := z_n$. This yields $F(z,\,u) = 0$, where $F : \mathbb{C} \times \mathbb{C} \to \mathbb{C}$ is given by

$$F(z,\,u) = e^{2\,z\,\tau}\,(i + u\,z + u\,\beta_1)\,(i + u\,z + u\,\beta_2) - (i + u\,z + u\,\gamma_1)\,(i + u\,z + u\,\gamma_2)\,. \tag{6.13}$$

A second-order Taylor expansion of $F$ provides

$$\begin{aligned} & F(0,\,0) = 0, \quad \frac{\partial\,F}{\partial\,z}(0,\,0) = -2\,\tau, \quad \frac{\partial\,F}{\partial\,u}(0,\,0) = i\,(\beta_1 - \gamma_1 + \beta_2 - \gamma_2)\,, \\ & \frac{\partial^2\,F}{\partial\,z^2}(0,\,0) = -\,(2\,\tau)^2\,, \frac{\partial^2\,F}{\partial\,z\,\partial\,u}(0,\,0) = 2\,i\,\tau\,(\beta_1 + \beta_2)\,, \frac{\partial^2\,F}{\partial\,u^2}(0,\,0) = 2\,(\beta_1\,\beta_2 - \gamma_1\,\gamma_2)\,. \end{aligned} \tag{6.14}$$

Since $\frac{\partial\,F}{\partial\,z}(0,\,0) \neq 0$, the implicit function theorem states that $(u,\,z(u))$ is a graph in a neighborhood of the origin, where $u \to z(u)$ is a holomorphic function. Differentiating $F(z(u),\,u) = 0$ yields

$$\frac{\partial\,F}{\partial\,z}\,z^{'} + \frac{\partial\,F}{\partial\,u} = 0, \tag{6.15}$$

and thus

$$z^{'}(0) = i\,\frac{\beta_1 - \gamma_1 + \beta_2 - \gamma_2}{2\,\tau}. \tag{6.16}$$

Since $z^{'}(0)$ is purely imaginary, one still cannot reach any conclusions about the monotonicity of $\Re\mathrm{e}\,(z)$. We therefore differentiate (6.15), which yields

$$\frac{\partial^2\,F}{\partial\,z^2}\left(z^{'}\right)^2 + 2\,\frac{\partial^2\,F}{\partial\,z\,\partial\,u}\,z^{'} + \frac{\partial^2\,F}{\partial\,u^2} + \frac{\partial\,F}{\partial\,z}\,z^{''} = 0. \tag{6.17}$$

Taking (6.14), (6.16) and (6.17), we obtain

$$z^{''}(0) = -\frac{\beta_1^2 - \gamma_1^2 + \beta_2^2 - \gamma_2^2}{2\,\tau} < 0. \tag{6.18}$$

Derivatives (6.16) and (6.18) are injected into the second-order Taylor series of $z$:

$$z(u) = i\,\frac{\beta_1 - \gamma_1 + \beta_2 - \gamma_2}{2\,\tau}\,u - \frac{1}{2}\,\frac{\beta_1^2 - \gamma_1^2 + \beta_2^2 - \gamma_2^2}{2\,\tau}\,u^2 + \mathcal{O}(u^3). \tag{6.19}$$

Based on $u = \tau\,/\,(n\,\pi)$, (6.11) and (6.19), the asymptotic expansion (6.9) is proved.

To prove the monotonicity of the real part of the asymptotic roots, we take $z = x + i\,y$. Taylor series (6.19) yields $x(0) = 0$, $x^{'}(0) = 0$ and $x^{''}(0) = z^{''}(0) < 0$.

As a result, $\Re\mathrm{e}\ (z)$ decreases with $u$ and $\Re\mathrm{e}\ (\Lambda_n) = \Re\mathrm{e}\ (z_n)$ increases with $n$ when $1\,/\,n \to 0$. Lastly, the monotonicity of $\Im\mathrm{m}\ (\Lambda_n)$ follows from (6.9). $\square$

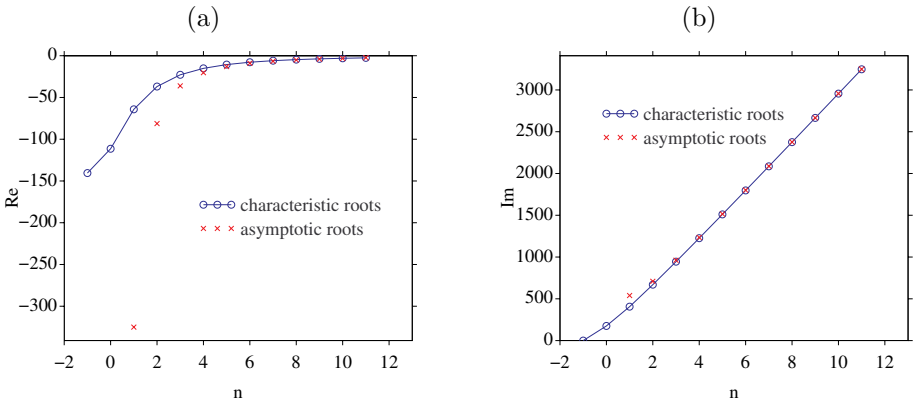


Fig. 3. Characteristic roots of (6.7): real parts (a) and imaginary parts (b). Blue circles and red crosses denote exact values and asymptotic values (6.9), respectively.

Two remarks about lemma 6.1:

- The holomorphic implicit function theorem used in the proof confirm that $z_n = \Lambda_n - i\,\frac{n\,\pi}{\tau}$ can be expressed in terms of arbitrary powers of $\frac{\tau}{n\,\pi}$.
- The monotonic behavior of characteristic roots (6.7) is valid only when sufficiently high values of $n$ are considered. No theoretical result is known in the case of small values of $n$. However, the results of numerical experiments have indicated that the monotonicity property is satisfied whatever the value of $n$.

In figure 3, asymptotic values (6.9) for $n = 1, \cdots, 10$ are compared with the characteristic roots in the upper part of the complex plane. The roots of (6.7) are computed numerically. The parameters are those used in further numerical experiments: (7.2) and $\alpha_2 - \alpha_1 = 30$ m. The predicted convergence properties are obtained. It is also worth noting that the first characteristic root (on the real line) and the second characteristic root are not included in the asymptotic expansion.

### 6.3. *Inverse linear operator*

Let us consider a monochromatic source $s(t) = s_1\, e^{i\,\omega\,t}$ in the linearized system (6.3). The source in (6.4) becomes

$$\mathbf{s}(t) = s_1 \begin{pmatrix} 1 \\ e^{-i\,\omega\,\tau} \end{pmatrix} e^{i\,\omega\,t} = \mathbf{s}_1\, e^{i\,\omega\,t}. \tag{6.20}$$

The solution of (6.5) with the source (6.20) is sought in the form of $\mathbf{y}(t) = \mathbf{y}_1\, e^{i\,\omega\, t}$, where $\mathbf{y}_1$ is a constant vector. Straightforward calculations give $\mathbf{y}_1 = \mathcal{L}^{-1}(\mathbf{s}(t)) = \mathbf{H}^{-1}(i\,\omega)\,\mathbf{s}_1$, where $\mathcal{L}^{-1}$ is the inverse operator of $\mathcal{L}$ in (6.5),

$$\mathbf{H}^{-1}(i\,\omega) = \frac{1}{h(i\,\omega)} \begin{pmatrix} i\,\omega + \beta_2 & -e^{-i\,\omega\,\tau}\,(i\,\omega + \gamma_2) \\ -e^{-i\,\omega\,\tau}\,(i\,\omega + \gamma_1) & i\,\omega + \beta_1 \end{pmatrix}, \tag{6.21}$$

and $h$ is the characteristic function in (6.7). The continuity of $\mathcal{L}^{-1}$ from $H^1_T$ into $H^1_T$ is a key step to study the nonlinear NDDE (3.2). Based on (6.21), the effect of $\mathcal{L}^{-1}$ on general sources in $H^p_T$ with an infinite number of harmonics is characterized in the next lemma.

**Lemma 6.2.** *The linear application $\mathcal{L}^{-1}$ is continuous from $H^p_T$ into $H^p_T$ if and only if*

$$\inf \left| \frac{h(i\,k\,\omega)}{k} \right| > 0, \qquad k \in \mathbb{Z}, \quad k \neq 0. \tag{6.22}$$

**Proof.** The continuity of $\mathcal{L}^{-1}$ is proved in $L^2_T$: since $\mathcal{L}^{-1}$ is a Fourier multiplier, continuity in $L^2_T$ entrains continuity in $H^p_T$. It remains to prove that $\sup |||\mathbf{H}^{-1}(i\,k\,\omega)|||$ is bounded. The matrix norm induced by the maximum norm in $\mathbb{C}^2$ is used. The notations $\lambda = i\,k\,\omega$, $\beta_{\max} = \max(\beta_1,\, \beta_2)$, and $\gamma_{\min} = \min(|\gamma_1|,\, |\gamma_2|)$ are introduced. The property $\beta_k > |\gamma_k|$, along with (6.21), yields

$$\begin{aligned} |||\mathbf{H}^{-1}(\lambda)||| &= \frac{1}{|h(\lambda)|}\, \max\left(|\lambda + \beta_1| + |\lambda + \gamma_1|,\, |\lambda + \beta_2| + |\lambda + \gamma_2|\right), \\ &\leq \frac{2}{|h(\lambda)|}\, \max\left(|\lambda + \beta_1|,\, |\lambda + \beta_2|\right), \\ &\leq \frac{2}{|h(\lambda)|}\, \max\left(|\lambda| + \beta_{\max}\right), \\ &\leq 2\left(1 + \frac{\beta_{\max}}{|\lambda|}\right) \Big/ \left|\frac{h(\lambda)}{\lambda}\right|. \end{aligned} \tag{6.23}$$

Likewise, we obtain

$$|||\mathbf{H}^{-1}(\lambda)||| \geq 2\left(1 + \frac{\gamma_{\min}}{|\lambda|}\right) \Big/ \left|\frac{h(\lambda)}{\lambda}\right|, \tag{6.24}$$

and hence $|||\mathbf{H}^{-1}(\lambda)||| \sim 2\left|\frac{h(\lambda)}{\lambda}\right|$ at high values of $|\lambda|$. Proving the continuity of $\mathcal{L}^{-1}$ therefore amounts to satisfying (6.22). □

Instead of studying the condition (6.22) directly, we first examine the lower bounds of $|h(\lambda)/\lambda^2|$, $\lambda \in i\,\mathbb{R}$, $\lambda \neq 0$. Based on (6.9), $|h(\lambda)/\lambda^2|$ is expected to be very close to zero near the projection $\lambda_n$ of the characteristic roots $\Lambda_n$ onto the imaginary axis, as seen in figure 4-(a). Using the asymptotic expansions given in

lemma 6.1, we obtain $\lambda_n = i\left(\frac{n\,\pi}{\tau} + \frac{\beta_1-\gamma_1+\beta_2-\gamma_2}{2\,n\,\pi}\right)$. A careful analysis of $|h(\lambda)/\lambda^2|$ along the imaginary axis and especially near $\lambda_n$ is therefore required, as investigated in the next lemma.

**Lemma 6.3.** *Some notations are introduced ($n \in \mathbb{Z}$):*

$$\begin{aligned} &\lambda = i\,(m+r)\,, \qquad m = \frac{n\,\pi}{\tau}, \qquad r \in \left[-\frac{\pi}{2\,\tau}, +\frac{\pi}{2\,\tau}\right], \\ &\lambda_n = i\,(m+r_n)\,, \qquad r_n = \frac{\beta_1-\gamma_1+\beta_2-\gamma_2}{2\,n\,\pi}, \end{aligned} \tag{6.25}$$

*and we assume $|\lambda| \gg 1$ (i.e. $|n| \gg 1$). The following estimates hold:*

- *for all $\varepsilon > 0$, there exists $C_0 > 0$ such that*

$$|\lambda - \lambda_n| > \frac{\varepsilon}{|m|} \;\Rightarrow\; \left|\frac{h(\lambda)}{\lambda^2}\right| > \frac{C_0}{|m|}. \tag{6.26}$$

- *if $\lambda = \lambda_n$, then there exists $C_1 > 0$ such that*

$$\left|\frac{h(\lambda_n)}{\lambda_n^2}\right| = \frac{\beta_1^2-\gamma_1^2+\beta_2^2-\gamma_2^2}{2\,m^2} + \mathcal{O}\left(\frac{1}{m^3}\right) \sim \frac{C_1}{m^2}. \tag{6.27}$$

**Proof.** We take positive values of $m$, i.e. positive imaginary values of $\lambda$; the case $m < 0$ can be treated in a similar way. Based on (6.25), it follows

$$\frac{1}{\lambda} = -\frac{i}{m} + \frac{i\,r}{m^2} + \mathcal{O}\left(\frac{1}{m^3}\right), \qquad \frac{1}{\lambda^2} = -\frac{1}{m^2} + \mathcal{O}\left(\frac{1}{m^3}\right). \tag{6.28}$$

From (6.7) and (6.28), we obtain Taylor series of increasing order

$$\begin{aligned} \frac{h(\lambda)}{\lambda^2} &= 1 + \frac{\beta_1+\beta_2}{\lambda} + \frac{\beta_1\,\beta_2}{\lambda^2} - e^{-2\,i\,\tau\,r}\left(1 + \frac{\gamma_1+\gamma_2}{\lambda} + \frac{\gamma_1\,\gamma_2}{\lambda^2}\right), \\ &= 1 - e^{-2\,i\,\tau\,r} + \mathcal{O}\left(\frac{1}{m}\right), \\ &= 1 - e^{-2\,i\,\tau\,r} - i\,\frac{\beta_1+\beta_2-e^{-2\,i\,\tau\,r}\,(\gamma_1+\gamma_2)}{m} + \mathcal{O}\left(\frac{1}{m^2}\right), \\ &= 1 - i\,\frac{\beta_1+\beta_2}{m} - \frac{\beta_1\,\beta_2}{m^2} + i\,\frac{(\beta_1+\beta_2)\;r}{m^2} \\ &\quad -e^{-2\,i\,\tau\,r}\left(1 - i\,\frac{\gamma_1+\gamma_2}{m} - \frac{\gamma_1\,\gamma_2}{m^2} + i\,\frac{(\gamma_1+\gamma_2)\;r}{m^2}\right) + \mathcal{O}\left(\frac{1}{m^3}\right). \end{aligned} \tag{6.29}$$

Three cases are distinguished.

Case 1: $\delta < |r| \leq \frac{\pi}{2\,\tau}$, where $\delta$ is an arbitrary positive real number. The $\mathcal{O}(1\,/\,m)$ series in (6.29); using the concave inequality of sinus function yields

$$\left|\frac{h(\lambda)}{\lambda^2}\right| > \left|1 - e^{2\,i\,\tau\,r}\right| > 2\,d\,\tau\,|r|,$$

where $d = 2\,/\,\pi > 0$. This gives the lower bound

$$\inf \left| \frac{h(\lambda)}{\lambda^2} \right| > 0, \tag{6.30}$$

independently of $m$.

Case 2: $\frac{\kappa}{m} \leq |r| \leq \delta$, where $\kappa$ is sufficiently large, for instance $\kappa = \frac{3}{2}\,\frac{\beta_1+|\gamma_1|+\beta_2+|\gamma_2|}{d\,\tau}$. Triangle inequality gives

$$\left| i\,\frac{\beta_1+\beta_2-e^{-2\,i\,\tau\,r}\,(\gamma_1+\gamma_2)}{m} \right| \leq \frac{\beta_1+|\gamma_1|+\beta_2+|\gamma_2|}{m}. \tag{6.31}$$

Using successively the concave inequality on sinus function, the assumption about $|r|$, the value of $\kappa$, and the inequality (6.31), results in

$$\begin{aligned} \left|1-e^{-2\,i\,\tau\,r}\right| &> 2\,d\,\tau\,|r|, \\ &> \frac{2\,d\,\tau\,\kappa}{m}, \\ &> 3\,\frac{\beta_1+|\gamma_1|+\beta_2+|\gamma_2|}{m}, \\ &\geq 2\,\frac{\beta_1+|\gamma_1|+\beta_2+|\gamma_2|}{m} + \left| i\,\frac{\beta_1+\beta_2-e^{-2\,i\,\tau\,r}\,(\gamma_1+\gamma_2)}{m} \right|. \end{aligned} \tag{6.32}$$

Equation (6.32) is then injected into the $\mathcal{O}(1\,/\,m^2)$ series of (6.29), which gives

$$\left| \frac{h(\lambda)}{\lambda^2} \right| > \frac{\beta_1+|\gamma_1|+\beta_2+|\gamma_2|}{m}. \tag{6.33}$$

Case 3: $|r| < \frac{\kappa}{m}$. Noting that $r = \mathcal{O}(1\,/\,m)$, it follows from (6.29) that

$$\begin{aligned} \frac{h(\lambda)}{\lambda^2} &= i\left(2\,\tau\,r - \frac{\beta_1-\gamma_1+\beta_2-\gamma_2}{m}\right) \\ &\quad + \left(2\,\tau^2\,r^2 - \frac{\beta_1\,\beta_2-\gamma_1\,\gamma_2}{m^2} + 2\,\tau\,r\,\frac{\gamma_1+\gamma_2}{m}\right) + \mathcal{O}\left(\frac{1}{m^3}\right), \\ &= i\left(2\,\tau\,r - \frac{\beta_1-\gamma_1+\beta_2-\gamma_2}{m}\right) + \mathcal{O}\left(\frac{1}{m^2}\right). \end{aligned} \tag{6.34}$$

Based on (6.34), we deduce that the value of $|h(\lambda)\,/\,\lambda^2|$ is minimum at $\lambda_n$ defined in (6.25). Injecting $\lambda_n$ into the $\mathcal{O}(1\,/\,m^3)$ series of (6.34) proves the estimate (6.27). On the other hand, let us take an arbitrarily small $\varepsilon > 0$, smaller than $\kappa$. The $\mathcal{O}(1\,/\,m^2)$ series given in (6.34) and the definition of $r_m$ given in (6.25) show that

$$\frac{h(\lambda)}{\lambda^2} = 2\,i\,\tau\,(r-r_m) + \mathcal{O}\left(\frac{1}{m^2}\right). \tag{6.35}$$

We therefore obtain

$$|r-r_n| > \frac{\varepsilon}{m} \;\Rightarrow\; \left| \frac{h(\lambda)}{\lambda^2} \right| > \frac{2\,\tau\,\varepsilon}{m}, \tag{6.36}$$

which proves (6.26). □

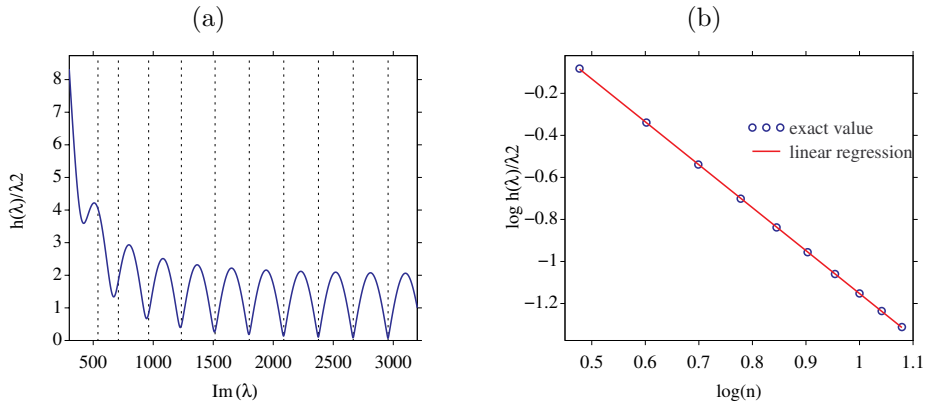


Fig. 4. (a): graph of $|h(\lambda)/\lambda^2|$ along the imaginary axis, where $h$ is the characteristic function (6.7); the dotted vertical lines denote the imaginary part $\lambda_n$ of the asymptotic expansion of $\Lambda_n$: see (6.9) and (6.25). (b): $|h(\lambda_n)/\lambda_n^2|$, where $n = 3, \ldots, 13$; the straight red line denotes the slope - 2 deduced from (6.27). In both (a) and (b), the physical parameters are based on (7.2), where $\alpha_2 - \alpha_1 = 30$ m.

The estimate (6.27) is illustrated in figure 4-(b). A log-log scale is used to see the $\mathcal{O}(1\,/\,m^2)$ behavior. As expected, the linear regression curve fitting $|h(\lambda_n)\,/\,\lambda_n^2|$ has a slope of - 2.

We can now address the main question of section 6: is the solution to the linear system of NDDE (6.3) as smooth as the source ? In the affirmative case, the existence and uniqueness of periodic solutions to the nonlinear system of NDDE (3.2) can be proved by applying standard tools, such as the implicit function theorem or a fixed point method; see section 6.5 for this topic. The following proposition shows that the answer is yes, under a suitable condition.

**Proposition 6.3 (Condition $\mathcal{P}$).** *Let us take the source (6.20), $m$ and $r_n$ defined in (6.25), and the interval*

$$E_\varepsilon = \bigcup_{n\in\mathbb{Z}} \left]m + r_n - \frac{\varepsilon}{m},\, m + r_n + \frac{\varepsilon}{m}\right[, \qquad \varepsilon > 0. \tag{6.37}$$

*The condition $\mathcal{P}$ is introduced: there exists $\varepsilon > 0$ such that for $k \in \mathbb{Z}$, $k\,\omega \notin E_\varepsilon$ except for a finite set of integers. The condition $\mathcal{P}$ is true if and only if $\mathcal{L}^{-1}$ is continuous from $H_T^p$ into $H_T^p$, whatever $p$. If $\mathcal{P}$ is false, then $\mathcal{L}^{-1}$ is continuous from $H_T^p$ into $H_T^{p-1}$.*

**Proof.** It is noticed that $|h(\lambda)\,/\,\lambda| \sim |h(\lambda)\,/\,\lambda^2|\,|m|$ when $\lambda$ is large. If $\mathcal{P}$ is true, then there exists $\varepsilon > 0$ such that $|\lambda - \lambda_n| > \frac{\varepsilon}{|m|}$, where $\lambda = i\,k\,\omega$. In this case, (6.26)

implies that $|h(\lambda)\,/\,\lambda| \sim C_1$. The bound (6.22) is therefore satisfied, which proves the case $\mathcal{P}$ true. If $\mathcal{P}$ is false, then it follows from (6.27) that $|h(\lambda)\,/\,\lambda| \sim C_0\,/\,m$. In this case, $\mathcal{L}^{-1}$ is not bounded in $H^p_T$ and one degree of regularity is lost: a small divisor problem arises here.[16,18] $\square$

### 6.4. *Diophantine condition*

In the following lemma, the condition $\mathcal{P}$ used in proposition 6.3 is expressed differently. This new formulation will be easier to check.

**Lemma 6.4.** *Condition $\mathcal{P}$ is equivalent to the condition $\mathcal{D}$ in definition 6.1.*

**Proof.** The notations (2.9), (3.8), (6.25) and (6.37) are used. Condition $\mathcal{P}$ is untrue iff there exists infinite sequences of integers $(n,\,k)$ satisfying

$$\left| k\,\omega - \left( \frac{n\,\pi}{\tau} + \frac{\beta_1 - \gamma_1 + \beta_2 - \gamma_2}{2\,n\,\pi} \right) \right| < \frac{\varepsilon\,\tau}{|n|\,\pi}. \tag{6.38}$$

Taking $\delta = \left(\frac{\tau}{\pi}\right)^2 \varepsilon$, equation (6.38) yields

$$\left| 2\,\theta - \left( \frac{n}{k} + \frac{2\,\zeta}{n\,k} \right) \right| < \frac{\delta}{|n\,k|}. \tag{6.39}$$

It follows that $\frac{1}{n} = \frac{1}{2\,\theta\,k} + o(\frac{1}{k})$, which is injected into (6.39). Since the inequality thus-obtained holds true with all $\delta > 0$, we obtain

$$\left| 2\,\theta - \left( \frac{n}{k} + \frac{\zeta}{\theta}\,\frac{1}{k^2} \right) \right| = o\left( \frac{1}{k^2} \right), \tag{6.40}$$

which is in line with (6.2) and proves the lemma. $\square$

We now prove the proposition 6.1, where it was stated that if $\theta = \tau\,/\,T \in \mathbb{Q}$, then condition $\mathcal{D}$ is true.

**Proof of proposition 6.1.** Let us assume that $\mathcal{D}$ is untrue. Since $\tau$ and $T$ are commensurable, there exist integers $p$ and $q$ such that $\theta = p\,/\,q$. Injecting this ratio into (6.2) proves that an infinite number of $(n,\,k)$ satisfy

$$2\,k\,p - n\,q = \frac{\zeta\,q^2}{k\,p} + o\left( \frac{1}{k} \right). \tag{6.41}$$

The left-hand side of (6.41) is a sequence of integers, whereas the right-hand side tends towards 0. Therefore there exists $k_0$ such that if $|k| > k_0$, then $2\,k\,p - n\,q = 0$. In this case,

$$\frac{\zeta\,q^2}{k\,p} + o\left( \frac{1}{k} \right) = 0 \iff \frac{\zeta\,q^2}{p} + o\,(1) = 0, \tag{6.42}$$

and thus $\frac{\zeta\,q^2}{p} = 0$, which is impossible. Consequently, $\mathcal{D}$ is true. $\square$

Proposition 6.1 suffices to show that $\mathcal{D}$ is true, and thus to prove the existence and uniqueness of a $T$-periodic solution in $H^1_T$ to (6.5): see proposition 6.3 and lemma 6.4. However, $\theta = \tau\,/\,T \in \mathbb{Q}$ is not necessary. The possible existence of a larger set of admissible $\theta$ is discussed in section 8.2.

### 6.5. *Nonlinear problem*

In section 6.4, theorem 6.1 was proved in the linear case (6.3). The aim of this section is to extend the proof to include the original nonlinear delay system (3.2), under the assumption that the source is small. Standard nonlinear analysis tools are used for this purpose.[4] Note that proposition 6.1, which was proved in section 6.4, is valid regardless of the size of the source.

**Proof of theorem 6.1.** With notations (6.4), the nonlinear NDDE system (3.2) is written

$$\mathbf{f}\left(\mathbf{y}(t)\right) = \mathbf{s}(t), \tag{6.43}$$

where the nonlinear function $\mathbf{f}$ depends on $f_1$ and $f_2$. Equation (6.43) is put in the form

$$\mathcal{L}\,\mathbf{y}(t) = \mathbf{g}\left(\mathbf{y}(t)\right) + \mathbf{s}(t), \tag{6.44}$$

where $\mathcal{L}$ is the linearized operator (6.5), and $\mathbf{g}$ is the Taylor remainder that satisfies $\mathbf{g}^{'}(\mathbf{0}) = \mathbf{0}$. It follows that $\mathcal{H}(\mathbf{y},\,\mathbf{s}) = \mathbf{0}$, where

$$\mathcal{H}(\mathbf{y},\,\mathbf{s}) = \mathbf{y}(t) - \mathcal{L}^{-1}\left(\mathbf{g}(\mathbf{y}(t) + \mathbf{s}(t)\right). \tag{6.45}$$

Under the Diophantine condition $\mathcal{D}$, proposition 6.3 and lemma 6.4 show that $\mathcal{L}^{-1}$ is continuous. Since $\frac{\partial\,\mathcal{H}}{\partial\,\mathbf{y}}(\mathbf{0},\,\mathbf{0}) = \mathbf{I} \neq \mathbf{0}$, the implicit function theorem can be applied, which concludes the proof. □

## 7. Numerical experiments

### 7.1. *Numerical methods*

**Time-domain method**. Two methods are developed for solving the linear elastodynamics models (2.1) with the jump conditions (2.2) and (2.5). The first one relies on direct numerical simulations, in the time-domain. A fourth-order finite-difference ADER scheme is used to integrate the conservation laws. The nonlinear jump conditions are discretized and injected in the scheme by an immersed interface method.[23] At each time step, the scheme gives $v$, $\sigma$, and $Y_k(t) = [u(\alpha_k,\,t)]$; numerical integration of $v$ also gives $u$ on the whole domain.

Numerical dispersion and numerical diffusion can be estimated by usual techniques of numerical analysis.[22] A sufficiently fine mesh is used to ensure that the numerical solutions can be taken to be the exact values. In counterpart, the time-domain simulations are not an efficient way to capture the periodic solutions, especially in the case of multiple cracks. As proved in section 6, indeed, the attractivity

of periodic solutions is small, and hence long-time integration is required to reach the periodic regime.

**Harmonic balance method**. When transient solutions are ignored, the harmonic balance method (HBM) is a very efficient numerical strategy. Infinite series (3.10) are truncated to $|n| \leq N$, and then they are injected into (3.2) and (3.5). It yields a $(4\,N + 2) \times (4\,N + 2)$ nonlinear system

$$\mathbf{F}(\mathbf{X}) = \mathbf{0}, \tag{7.1}$$

where $\mathbf{X}$ is the vector of $4\,N + 2$ Fourier coefficients.

In the limit case of an infinitesimal forcing level, (7.1) becomes a linear system the solution of which is known analytically: see section 4.1. In the general nonlinear case, no exact solution of (7.1) is known and numerical methods are required. We have therefore developed computer algebra tools for exactly determining $\mathbf{F}$ and its Jacobian $\mathbf{J}$. With these programs, high orders (such as $N = 40$) can be reached in a few seconds on a Pentium IV (3 GHz).

Once $\mathbf{F}$ and $\mathbf{J}$ are formally determined, a Newton-Raphson method is applied. Some care must be taken about the initial guess: at large forcing levels, numerical experiments have shown that multiple roots of (7.1) can occur. To prevent spurious solutions from occurring, a basic continuation method is adopted[27]:

- a uniform forcing scale is used, ranging from a small $v_0^{(0)}$ up to the forcing level of interest;
- the exact solution $\mathbf{X}^{(0)}$ is computed for $v_0^{(0)}$;
- the forcing level is incremented, and $\mathbf{X}^{(0)}$ is then used as the initial value in the Newton-Raphson algorithm to compute $\mathbf{X}^{(1)}$, and so on.

In each of the simulations obtained by HBM, preliminary convergence studies are performed to ensure that a sufficiently large number of Fourier modes are present. Model 1 of contact (3.5) is used, and the source is monochromatic (3.7).

### 7.2. *Scattered waves*

In a first series of numerical experiments, we focus on the dynamical behavior of the scattered waves. A 400 m domain is considered, with two cracks at $\alpha_1 = 170.1$ m and $\alpha_2 = 270.1$ m. The physical parameters are

$$\begin{cases} \rho_0 = \rho_1 = \rho_2 = 1200 \ \text{kg.m}^{-3}, & K_1 = K_2 = 1.3\,10^9 \ \text{kg.m}^{-1}.\text{s}^{-2}, \\ c_0 = c_1 = c_2 = 2800 \ \text{m.s}^{-1}, & d_1 = d_2 = 6.1\,10^{-6}\,\text{m}. \end{cases} \tag{7.2}$$

A source at $x_s = 50$ m emits a purely sinusoidal wave with a frequency of 50 Hz and an amplitude of elastic velocity $v_0$. Values of $v_0$ are considered from $10^{-4}$ m/s to $5\,10^{-3}$ m/s. The latter value corresponds to a maximum strain $\varepsilon = v_0/c_0 \approx 10^{-6}$, so that the linear elastodynamics models (2.1) is still valid.[1]

Figure 5 shows snapshots of $u$ at $t_f = 0.34$ s, obtained by time-domain methods. The mean spatial values $\overline{u}_k$ of the displacements in each of the subdomains are denoted by horizontal dotted lines. Three observations are done:

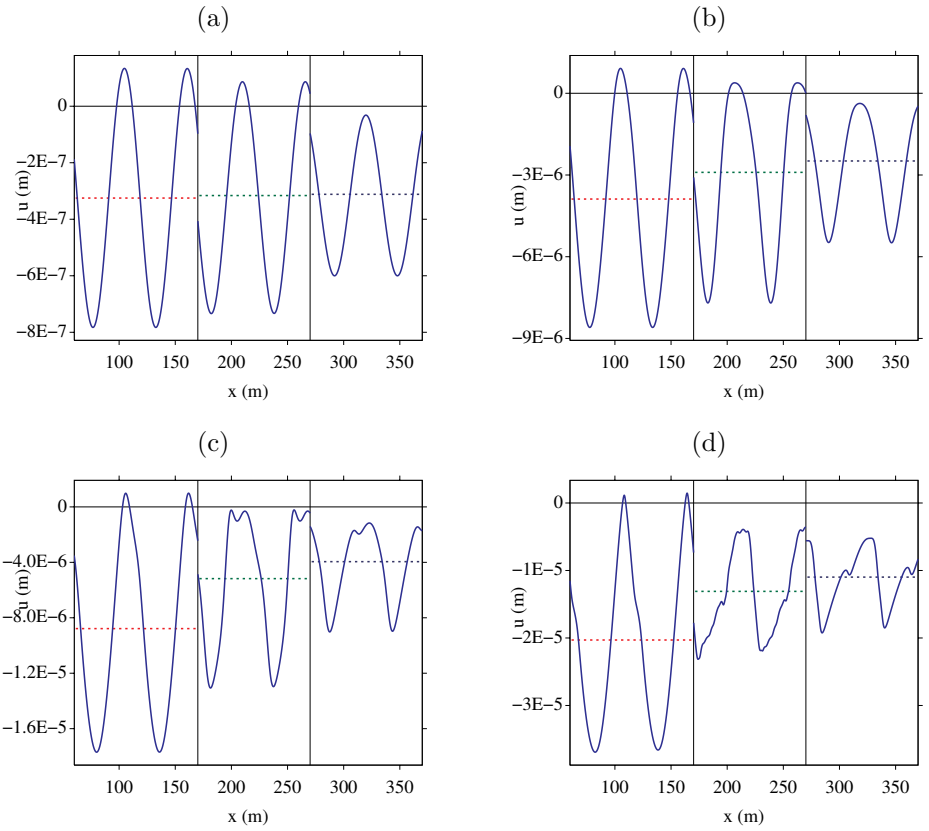


Fig. 5. Snapshots of the elastic displacement $u$ obtained with model 1 (2.7) and various amplitudes $v_0$ of the incident elastic velocity in (3.7): $10^{-4}$ m/s (a), $10^{-3}$ m/s (b), $2\,10^{-3}$ m/s (c) and $5\,10^{-3}$ m/s (d). The vertical solid lines denote the locations of the cracks. The red, green and navy dotted horizontal lines denote the mean spatial value $\overline{u}$ of the elastic displacement in each subdomain.

- a periodic solution is found to be reached in each subdomain;
- the scattered displacements are distorted when the forcing level increases;
- null or positive jumps in $\overline{u}_k$ occur across the cracks; null jumps occur at small forcing levels $v_0$ (a), whereas the jumps increase with the forcing level (b,c,d).

The positive jumps in $\overline{u}_k$ mentioned above are equal to the mean temporal value of $Y_k$, and they amount to a mean dilatation of the crack at $\alpha_k$.

The time histories of $Y_k$ are presented in the left row of figure 6. Logically, $Y_k$ are null until the wave emitted by the source has reached the first crack at $\alpha_1$, and subsequently, at $\alpha_2$. At small forcing levels (a), $Y_k$ are sinusoids centered around a null mean value. As $v_0$ increases, $Y_k$ are distorted and centered around an increasing positive mean value. The periodic regime also takes longer to be established. Lastly,

it is observed that the minimum values of $Y_k$ decrease and are bounded below by $-d_1 = -d_2$, as shown in (e); this property was required by the model (2.4).

The configuration space $(Y_1, Y_2)$ is shown in the right row of figure 6. The data between $[t_f - T, t_f]$ have been extracted and presented in the form of a continuous red line: at the forcing levels tested, this line is closed, which indicates that a periodic limit cycle has been reached. At small forcing levels (b), a centered elliptic limit cycle is observed, as predicted by the linear theory of oscillators. As $v_0$ increases, the limit cycle becomes more complex, and even crosses itself (f).

### 7.3. *Mean dilatations of the cracks*

In a second series of numerical experiments, we focus on the mean dilatation of the cracks. This phenomenon was observed numerically in figure 5, and it was analyzed quantitatively in section 4 by a perturbation method.

Figures 7 and 8 illustrate the proposition 4.1. The parameters are the same here as in (7.2). The reference solutions are obtained using the harmonic balance method (section 7.1), with $N = 20$ Fourier modes. In figure 7, the forcing level varies from $v_0 = 10^{-4}$ m/s to $v_0 = 2\,10^{-3}$ m/s, where strong nonlinear effects exist. The parameters are the same than in the previous section, giving $\theta = \tau \,/\, T \approx 0.535$. The approximate solution (4.15) corresponds to a straight line with slope +2, and it provides an excellent estimate of $\overline{Y_k}$ at small forcing levels. At higher values of $v_0$, a slight shift between $\overline{Y_k}$ and (4.15) occurs, but good agreement is still observed.

In figure 8, the parametric study is performed in terms of $\theta$, with $\varphi = 2\,\pi\,\theta$ in (4.9) and $\theta \in ]0,\, 1]$. At small forcing level (a), the approximate solution (4.15) provides an excellent estimate of $\overline{Y_k}$. At large forcing levels, the agreement is naturally less accurate. In both cases, it is observed that $\overline{Y_k}$ are 0.5-periodic in $\theta$, as stated in remark 3.2. This does not mean that $Y_k$ are 0.5-periodic: in practice, the $Y_k$ are only 1-periodic, as stated in remark 3.1.

This property can be proved at small forcing levels. From (4.15) and (4.9), it follows that only $2\,n\,\varphi$ is involved in $\overline{Y_k}$, and not $n\,\varphi$: the perturbation analysis therefore confirms the 0.5-periodicity of $\overline{Y_k}$ in terms of $\theta$. This property seems to also hold at large forcing levels, as indicated by many other simulations; however, no rigorous proof of this assumption has been obtained so far.

A final (erroneous) property might seem to be suggested by figure 8: it can be observed that $\overline{Y_1}$ and $\overline{Y_2}$ intersect at $\theta = 0.5$ and $\theta = 1$. In general, this property is untrue. It is satisfied iff the media are identical ($\rho_0 = \rho_1 = \rho_2$, $c_0 = c_1 = c_2$) and if the cracks are identical ($K_1 = K_2$, $d_1 = d_2$). This can easily be checked, taking theorem 5.1, theorem 5.2 and proposition 5.1 proposed in section 5.

### 7.4. *Special case $\theta = n \,/\, 2$*

In this section, we illustrate numerically the special case investigated in section 5, where $\Omega_1$ contains $n \,/\, 2$ wavelengths ($n \in \mathbb{N}$).

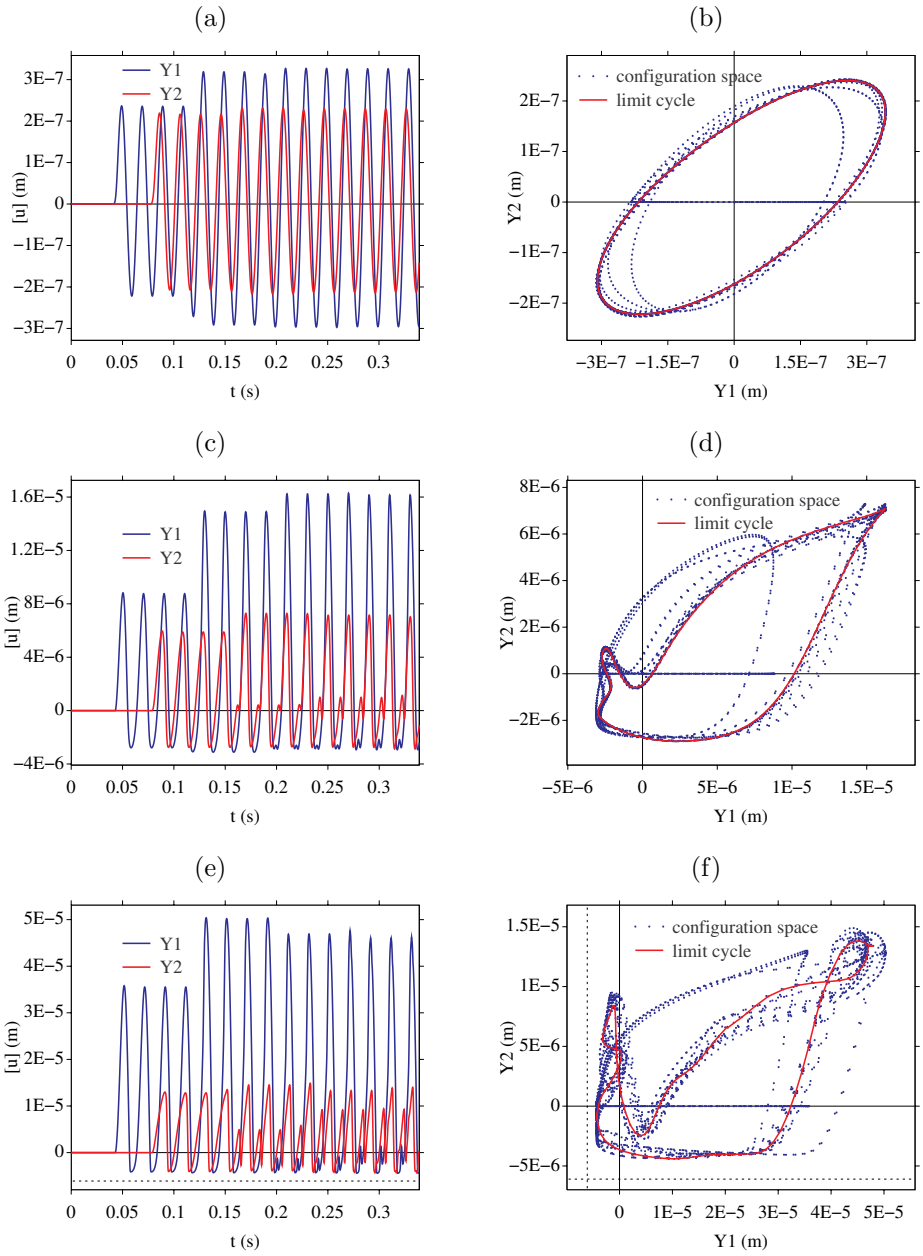


Fig. 6. Time histories of $Y_k = [u(\alpha_k, t)]$ (left row) and configuration space $(Y_1, Y_2)$ (right row) in the case of model 1 (2.7) and various amplitudes $v_0$ of the incident elastic velocity: $10^{-4}$ m/s (a-b), $2\,10^{-3}$ m/s (c-d) and $5\,10^{-3}$ m/s (e-f). In (e-f), the dotted lines denotes $-d_1 = -d_2$.

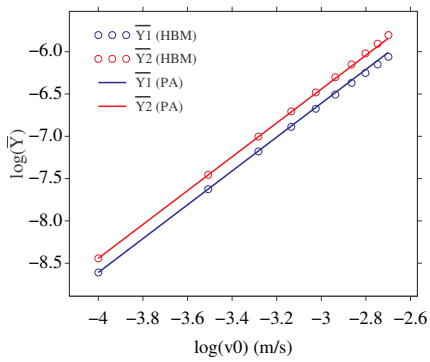


Fig. 7. Log-log evolution of $\overline{Y_k}$ in terms of the forcing amplitude $v_0$. Circle: harmonic balance method (HBM). Solid line: perturbation analysis (PA), Eq. (4.17).

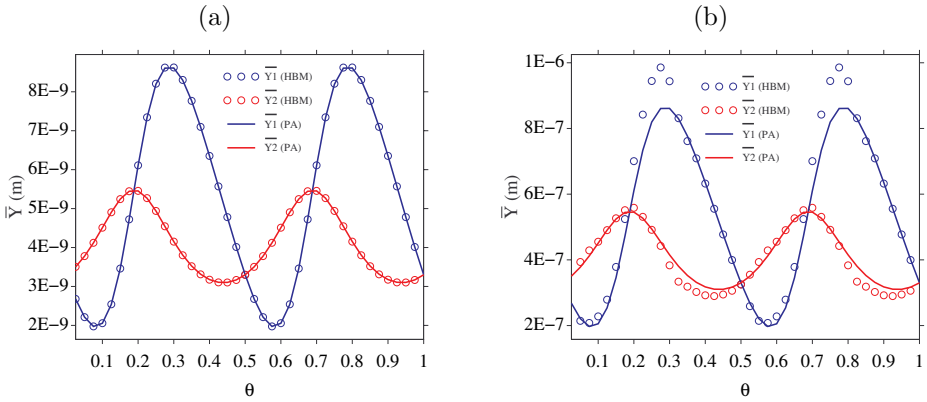


Fig. 8. Evolution of $\overline{Y_k}$ in terms of the ratio $\theta = \tau\,/\,T$. (a): $v_0 = 10^{-4}$ m/s; (b): $v_0 = 10^{-3}$ m/s. Circle: harmonic balance method (HBM). Solid line: perturbation analysis (PA), Eq. (4.17).

Theorems 5.1 and 5.2 are illustrated in figure 9. The simulations are performed by the harmonic balance method (section 7.1). The densities and celerities are the same as in (7.2); the parameters of the cracks are

$$\begin{aligned} K_1 &= 10^9 \ \text{kg.m}^{-1}.\text{s}^{-2}, \qquad d_1 = 6\,10^{-6}\,\text{m}, \\ K_2 &= 2\,10^9 \ \text{kg.m}^{-1}.\text{s}^{-2}, \qquad d_2 = 3\,10^{-6}\,\text{m}. \end{aligned} \tag{7.3}$$

Since the cracks are not identical, proposition 5.1 implies that $G \neq I$: the shapes of $y_2$ and $y_1$ are therefore not the same. If $\theta = 1$ (b), the respective minima and maxima of $y_1$ and $y_2$ are located at the same places, whereas a time shift $T/2$ occurs if $\theta = 0.5$ (a).

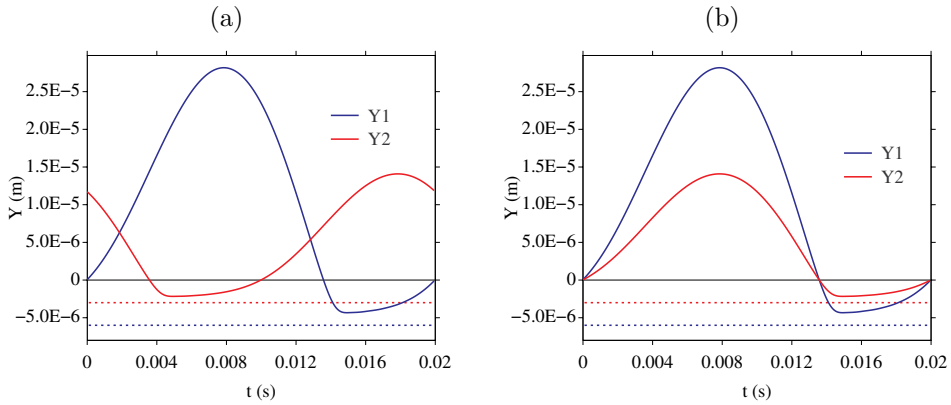


Fig. 9. Time history of $Y_1$ and $Y_2$ during one period, with $\theta = 0.5$ (a) and $\theta = 1$ (b): see theorems 5.1 and 5.2. Parameters: model 1 (3.5), sinusoidal forcing (3.7) with $v_0 = 5\,10^{-3}$ m/s. The horizontal blue and red dotted lines denote the lower bounds $-d_1$ and $-d_2$, respectively.

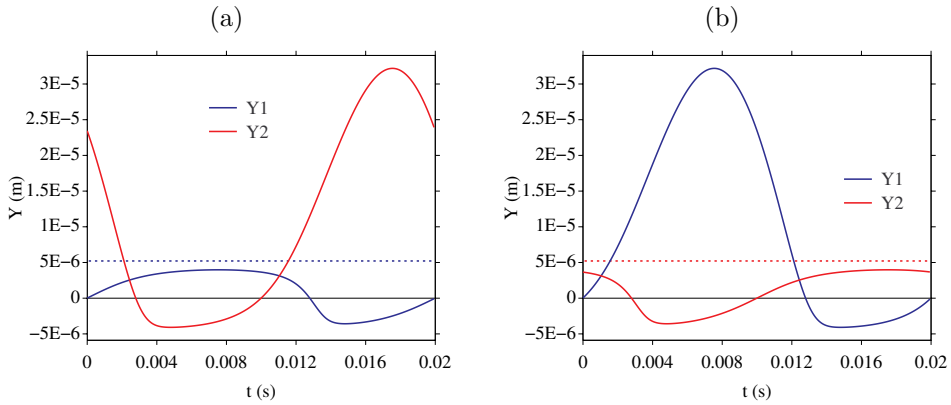


Fig. 10. Upper bounds if $\theta = 0.5$: see corollary 5.1. (a): $K_2\,d_2 < K_1\,d_1 \Rightarrow y_{1\,\max} < +\infty$; (b): $K_2\,d_2 > K_1\,d_1 \Rightarrow y_{2\,\max} < +\infty$. The horizontal blue or red dotted lines denote the upper bounds of the solutions $y_{i\,\max}$.

Corollary 5.1 is illustrated in figure 10, taking $\theta = 0.5$ and a sinusoidal forcing with amplitude $v_0 = 5\,10^{-3}$ m/s (3.7). The densities and celerities are the same as in the tests presented in section 7.2; the parameters of the cracks are

$$\begin{aligned} K_1 &= 1.3\,10^9 \ \text{kg.m}^{-1}.\text{s}^{-2}, \quad d_1 = 6.1\,10^{-6}\,\text{m}, \\ K_2 &= 2.5\,10^9 \ \text{kg.m}^{-1}.\text{s}^{-2}, \quad d_2 = 8.1\,10^{-6}\,\text{m}, \end{aligned} \tag{7.4}$$

such that $K_1\,d_1 < K_2\,d_2$ (a). Another set of parameters is also obtained by permuting indexes 1 and 2, hence $K_1\,d_1 > K_2\,d_2$ (b). In both cases, a positive horizontal

asymptote is observed in $y_1$ (a) and $y_2$ (b), as predicted by corollary 5.1. Similar figures (not shown here) are observed when $\theta = 1$. Lastly, the previously used parameters (7.3) yield $K_1\, d_1 = K_2\, d_2$: as predicted by corollary 5.1, no upper bound is observed in figure 9.

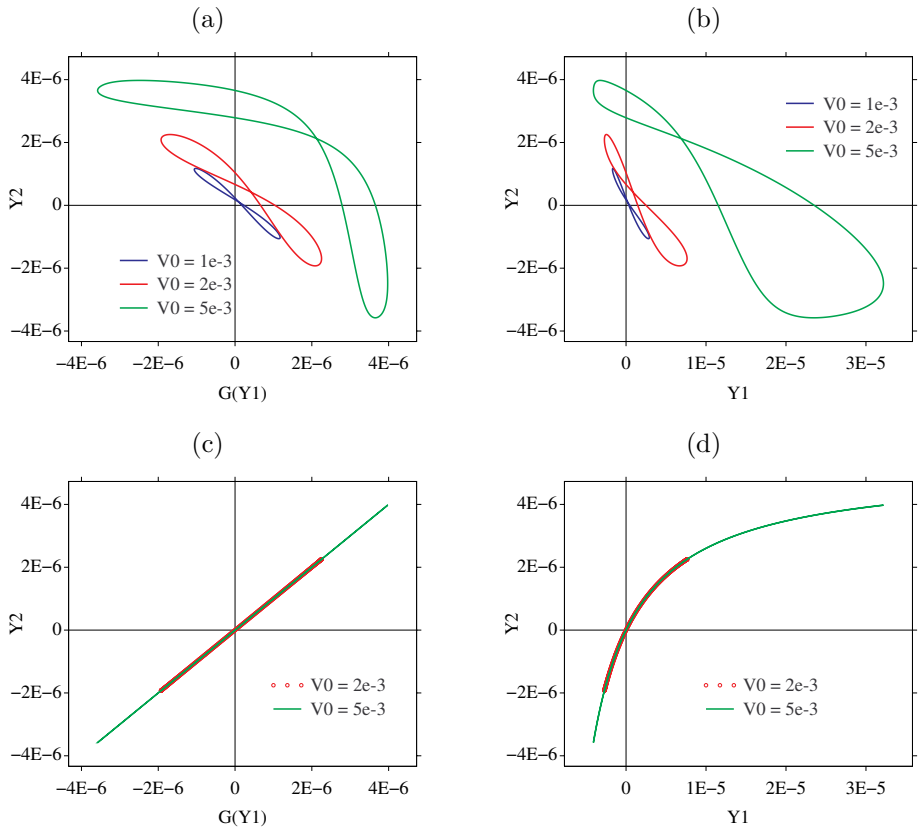


Fig. 11. Configuration space $\Gamma_G$ (a-c) and $\Gamma_I$ (b-d) with $\theta = 0.5$ (a-b) and $\theta = 1$ (c-d): see proposition 5.2. Amplitude $v_0$ of the sinusoidal forcing (3.7): $10^{-3}$ m/s, $2\,10^{-3}$ m/s, $5\,10^{-3}$ m/s.

Proposition 5.2 is illustrated in figure 11, for various levels of $v_0$ in (3.7). The physical parameters are given in (7.4), and thus proposition 5.1 yields $G \neq I$. If $\theta = 0.5$ (a-b), the symmetry properties of $\Gamma_G$ observed in (a) are lost by $\Gamma_I$ (b), where the configuration space is $(y_1, y_2)$. If $\theta = 1$, $\Gamma_G$ will be a straight line (c), whereas $\Gamma_I$ is shown on the graph of $G$ (d).

## 8. Conclusion

### 8.1. *Physical implications*

The property 3.2 and the proposition 4.1 extend to two cracks the results obtained with one crack, in particular the theorem 6-3 presented in Ref. 19. In the present study, we have proved that the jumps of elastic displacement oscillate around positive mean values $\overline{Y_k}$, which amount to mean dilatations of each crack. These dilatations increase quadratically with the forcing level $v_0$. Lastly, estimates of $\overline{Y_k}$ are proposed in (4.15), in the limits of a small forcing. Each term in (4.15) has a clear and separate physical significance:

- $\mathcal{F}_k^{''}(0) \,/\, d_k$ is a feature of the nonlinear crack, involving the local concavity of the contact law at the origin $\mathcal{F}_k^{''}(0)$ and the maximum allowable closure $d_k$;
- $\frac{v_0}{\omega}$ denotes the amplitude of the source;
- $X_{k(1)}^{(n)}$ corresponds to the mechanical oscillation of the crack in the linear regime;
- $\frac{s_n}{n}$ involves the Fourier spectrum of the source.

An application of this study is to characterize real cracks by non-destructive techniques. Knowing the maximal allowable closure of the cracks $d_k$ is crucial in geomechanics and geohydrology, where it is linked to the transport of fluids across fractured rocks.[3] If the source and the physical parameters around the cracks are known, then measuring the mean dilatations $\overline{Y_k} = \overline{[u(\alpha_k,\, t)]}$ provides an estimate of $|\mathcal{F}_k^{''}(0)| \,/\, d_k$ in(4.15). The stiffnesses $K_k$ is involved in (4.15), via the equations (2.9) and (4.9); they are obtained by usual acoustic methods.[30] The only difficulty is thus to measure $\overline{[u(\alpha_k,\, t)]}$.

For this purpose, two methods exist. The first one is to measure the dilatation of the crack mechanically with strain gauges around the crack.[21] The second method is to measure the scattered elastic waves. From the reflection or transmission coefficients, one can infer the mean jumps of elastic displacements; see for instance section 7-2 of Ref. 19 for details in the case of a single crack.

### 8.2. *Future lines of investigation*

**Periodic solutions**. The physical observables mentioned in section 8.1 depend on the existence and uniqueness of periodic solutions to the nonlinear NDDE (3.2)-(3.3). The results obtained along section 6 suffer from two limitations:

- in theorem 6.1, existence and uniqueness have been proven for small source under a diophantine condition;
- the sufficient condition in proposition 6.1 holds for a dense set of $\theta = \tau \,/\, T$, where $\tau$ is the travel time between the cracks, and $T$ is the period of the source. The size of the subset of $\mathbb{R}$ satisfying the necessary and sufficient condition $\mathcal{D}$ is not known.

We do not know whether these restrictions reflect reality (for instance, a lost of uniqueness in the case of large sources), or whether they are simply induced by the technical tools used in the proofs. As an argument in favor of the latter "technical" hypothesis, let us consider the special case $\theta = n\,/\,2$ ($n \in \mathbb{N}$) investigated in section 5. In this case, theorems 5.1 and 5.2 ensure the existence and uniqueness of the solution whatever the amplitude of the source, whereas theorem 6.1 does not. As a second argument, many numerical experiments have been performed with large forcing and various values of $\theta$ (in practice, rational values of $\theta$ are considered numerically): existence of a periodic regime has always been observed.

To be able to clear up this point, other techniques are probably required. Schauder's fixed point method could be used to prove the existence whatever the amplitude of the source, but the uniqueness would be lost. To prove the existence and uniqueness with a full set of ratios $\theta$, the Nash-Moser theorem[16,18] could be applied, but the results would still be restricted to small sources.

**Multiple cracks**. Wave scattering by a large number $N$ of nonlinear cracks is frequently involved in real applications. Physically relevant processes are expected: wave localization, band-pass behavior, chaos, etc.[32] The reduction of model followed in section 2.2 should provide a system of $N$ coupled nonlinear neutral delay differential equations. The method used in section 6 is probably intricate when $N$ large, but the NDDE system remains probably useful if it is combined with other approaches.

A promising strategy is to take advantage of the conservation of mechanical energy.[22] This energy is the sum of two terms: the mechanical energy of elastic waves outside the cracks, and the potential energy of nonlinear deformation of the cracks. From the properties of these terms, it may be possible to deduce qualitative results about the solution.

**Complex media**. Along this paper, the focus was put on the mechanical behavior of cracks; therefore the elementary framework of linear elastodynamics was chosen. This framework is sufficient for a large class of problems encountered in real applications, at least qualitatively, but one can wonder whether more complex models could be used and analyzed with the tools proposed along this article.

Some preliminary remarks can be done on this topic. Our approach relies on the transformation of the system (2.1) coupled with the jump conditions (2.2) and (2.5) into the system of neutral delay differential equations (2.10). This reduction, which is performed in proposition 2.1, requires to express the field at $\alpha_1^+$ in terms of the field at $\alpha_2^-$, and reciprocally.

In other words, our approach could be extended to media where the method of characteristics holds. For instance, it is the case of linear viscoelasticity and of linear poroelasticity. The generalization to nonlinear constitutive laws, leading to nonlinear hyperbolic systems, is more complex and requires a deeper exam.

**Acknowledgments**. This research was supported by the GdR 2501, CNRS, France. The authors are grateful to Gérard Iooss for discussions about small divisors, Diophantine conditions and the Nash-Moser theorem. We also thank Joël Piraux, Martine Pithioux, Bernard Rousselet and Christophe Vergez for their comments on the manuscript. Lastly, we thank Jessica Blanc for her reading, and Gary Burkhart for his advices on scientific communication.

## References

1. J. D. Achenbach, *Wave Propagation in Elastic Solids*, North-Holland Publishing (Amsterdam, 1973).
2. J. D. Achenbach and A. N. Norris, Loss of specular reflection due to nonlinear crack-face interaction, *J. NonDest. Eval.* **3** (1982) 229-239.
3. P. M. Adler, *Fractures and Fracture Networks*, Theory and Applcations of Transport in Porous Media (Kluwer Academic Publishers, 1999).
4. S. Alinhac and P. Gérard, *Pseudo-differential operators and the Nash-Moser theorem*, Graduate Studies in Mathematics 82 (2007).
5. S. C. Bandis, A. C. Lumsden and N. R. Barton, Fundamentals of rock fracture deformation, *Int. J. Rock Mech. Min. Sci. Geomech. Abstr.* **20** (1983) 249-268.
6. A. Bellen and M. Zennaro, *Numerical Methods for Delay Differential Equations*, Numerical Mathematics and Scientific Computation (Oxford University Press, 2003).
7. R. Bellman and K. Cooke, *Differential Difference Equations*, Academic Press (1963).
8. S. Biwa, S. Nakajima and N. Ohno, On the acoustic nonlinearity of solid-solid contact with pressure dependent interface stiffness, *ASME J. Appl. Mech.* **71** (2004) 508-515.
9. P. Das and N. Misra, A necessary and sufficient condition for the solution to a functional differential equation to be oscillatory, *J. Math. Anal. Appl.* **205** (1997) 78-87.
10. O. Diekmann, S. A. van Gils, S. M. Verduyn Lunel and H. O. Walther, *Delay Equations: Functional, Complex and Nonlinear Analysis*, Applied Mathematical Sciences 110 (Springer Verlag 1995).
11. L. H. Erbe, G. Kong and B. G. Zhang, *Oscillation Theory for Functional Differential Equations*, Monographs and Textbooks in Pure and Applied Mathematics 190 (Marcel-Dekker 1995).
12. K. Gopalsamy, *Stability and Oscillations in Delay Differential Equations of Population Dynamics*, Mathematics and its Applications (Kluwer Academic Publisher 1992).
13. I. Gyori and G. Ladas, *Oscillation Theory of Delay Differential Equations*, Oxford Mathematical Monographs (Oxford University Press, 1991).
14. J. K. Hale and H. Koçak, *Dynamics and Bifurcations*, Texts in Applied Mathematics (Springer-Verlag, 1991).
15. J. K. Hale and S. M. Verduyn Lunel, *Introduction to Functional Differential Equations*, Applied Mathematical Sciences 99 (Springer Verlag 2003).
16. R. S. Hamilton, The inverse function theorem of Nash and Moser, *Bull. Amer. Math. Soc.* **7-1** (1982) 65-222.
17. J. H. Hubbard and B. H. West, *Differential Equations: a Dynamical System Approach*, Texts in Applied Mathematics (Springer-Verlag, 1991).
18. G. Iooss and P. Plotnikov, Small divisor problem in the theory of three-dimensional water gravity waves, *Memoirs of AMS* **200-940** (2009).
19. S. Junca and B. Lombard, Dilatation of a one-dimensional nonlinear crack impacted by a periodic elastic wave, *SIAM J. Appl. Math.* **70-3** (2009) 735-761.
20. S. Junca and B. Rousselet, The method of strained coordinates for vibrations with weak unilateral springs, *IMA J. App. Math.* **76-2** (2011) 251-276.

21. B. A. Korshak, I. Y. Solodov and E. M. Ballad, DC effects, sub-harmonics, stochasticity and "memory" for contact acoustic non-linearity, *Ultrasonics* **40** (2002) 707-713.
22. B. Lombard, Modélisation numérique de la propagation et de la diffraction d'ondes mécaniques, HDR thesis, Université de la Méditerrané (2010), `http://tel.archives-ouvertes.fr/docs/00/44/88/97/PDF/Hdr.pdf`.
23. B. Lombard and J. Piraux, Modeling 1-D elastic P-waves in a fractured rock with hyperbolic jump conditions, *J. Comput. App. Math.* **204** (2007) 292-305.
24. B. Lombard and J. Piraux, Propagation of compressional elastic waves through a 1-D medium with contact nonlinearities, *Springer Proceedings in Physics* (2009)317-327.
25. O. Lopes, Forced oscillations in nonlinear neutral differential equations, *SIAM J. Appl. Math.* **29-1** (1975) 196-207.
26. B. Malama and P. H. Kulatilake, Models for normal fracture deformation under compressive loading, *Int. J. Rock Mech. Min. Sci.* **40** (2003) 893-901.
27. A. H. Nayfeh and B. Balachandran, *Applied Nonlinear Dynamics*, Wiley series in nonlinear science (John Wiley & Sons, 1995).
28. I. Niven, *Diophantine approximations*, Interscience Publishers (John Wiley & Sons, 1963).
29. N. Parhi and R. N. Rath, Oscillation criteria for forced first order neutral differential equations with variable coefficients, *J. Math. Anal. Appl.* **256** (2001) 525-541.
30. L. Pyrak-Nolte, L. Myer and N. Cook, Transmission of seismic waves across single natural fractures, *J. Geophys. Res.* **95** (1990) 8617-8638.
31. J. M. Richardson, Harmonic generation at an unbonded interface: I. Planar interface between semi-infinite elastic media, *Int. J. Eng. Sci.* **17** (1979) 73-85.
32. O. Richoux, C. Depollier and J. Hardy, Propagation of mechanical waves in a one-dimensional nonlinear disordered lattice, *Physical Review E* **73** (2006) 026611.
33. S. I. Rokhlin and Y. J. Wang, Analysis of boundary conditions for elastic wave interaction with an interface between two solids, *J. Acoust. Soc. Am.* **89-2** (1991) 503-515.
34. J. Shen and R. Liang, Periodic solutions for a kind of second-order neutral functional differential equations, *Appl. Math. Comput.* **190** (2007) 1394-1401.
35. I. Y. Solodov, Ultrasonics of non-linear contacts: propagation, reflection and NDE-applications, *Ultrasonics* **36** (1998) 383-390.
36. G. Scarella, Etude théorique et numérique de la propagation d'ondes en présence de contact unilatéral dans un milieu fissuré, PhD thesis, Paris IX (2009), `http://tel.archives-ouvertes.fr/docs/00/04/68/76/PDF/tel-00006272.pdf`.
37. X. F. Zhou, J. Liang and T. J. Xiao, Asymptotic stability of the zero solution for degenerate retarded differential equations, *Nonlinear Analysis* **70** (2009) 1415-1421.